FAULT CHARACTERIZATION USING INDUCED ELECTRIC CURRENTS PRESUMED TO UNDERGO ANOMALOUS DIFFUSION IN MASON, TEXAS

A Thesis

by

BLAINE CULLEN MURPHY

Submitted to the Office of Graduate and Professional Studies of
Texas A&M University
in partial fulfillment of the requirements for the degree of

MASTER OF SCIENCE

Chair of Committee,	Mark Everett
Co-Chair of Committee,	David Sparks
Committee Member,	Wayne Saslow
Head of Department,	Rick Giardino

August 2014

Major Subject: Geophysics

ABSTRACT

A tensorial (9-component) controlled source electromagnetic survey over an oblique slip fault in Mason County, Texas was acquired and the data were analyzed in order to characterize the structure of the fault and observe the diffusion of the induced currents in a fractured medium. The fault juxtaposes a Cambrian sandstone against Precambrian granite and both are highly resistive media that are not generally conducive to electromagnetic surveys.

The loop-loop method used in this project induces an eddy current system in the subsurface that moves down and out like a smoke ring. The eddy currents generate a transient magnetic field that is recorded by the receiver loop, which is stepped out from the transmitter loop at various offsets. The 9-component data set includes responses with the 3 orthogonal source orientations and 3 similar receiver orientations at each offset, and data were recorded over the fault zone along two oppositely-directed profiles.

Induced currents were presumed to diffusive anomalously in the presence of a geologically rough medium, in this case the fractured subsurface of the fault zone. Classic diffusion corresponding to a continuously differentiable medium would result in a decay of the received signal according to a $t^{-5/2}$ power law. Deviation of the power law decay from a -5/2 slope indicates anomalous diffusion of the subsurface eddy current system. A faster decay in the transient response at long offsets was observed, and it suggests highly resistive fractures in the fault zone at depth. A shallower decay at near offset, and for the shallower-probing vertical co-planar orientation, suggests more conductive fractures in the near surface A higher resolution 3-dimensional survey is required to rigorously test whether induced currents indeed

undergo anomalous diffusion in a rough geological medium.

DEDICATION

I dedicate this thesis project to my parents Lonnie and Barbara, and my brother Michael. They have been a continuous source of support and motivation throughout both my undergraduate and graduate studies.

ACKNOWLEDGEMENTS

Firstly, I would like to thank my family for their love and support. They have always encouraged me in my studies and inspired me to work hard in all of my endeavors.

I would like to thank my adviser Dr. Mark Everett for taking me on as a graduate student. I greatly appreciate the opportunity he has given me, his guidance during my graduate studies, and his assistance with this thesis project.

I would also like to thank my committee co-chair Dr. David Sparks, as well as Dr. Wayne Saslow and Dr. Joseph Ross for their insight and expertise. In addition, I appreciate the assistance of Dr. Mike Heaney with mapping the field site.

I would like to acknowledge the Berg-Hughes Center for the fellowship I received my first year of graduate school. It was a tremendous help while furthering my education.

Finally, I would like to thank Akhil Amara, Patrick Wagner, Oscar Vasquez, and Nick McDaniel for the help in the field acquiring the electromagnetic data.

TABLE OF CONTENTS

Page

LIST OF FIGURES

FIGURE Page

LIST OF TABLES

TABLE Page

1. INTRODUCTION

Electromagnetic induction surveys were conducted over a fault in Mason County in central Texas. Several previous geological and geophysical studies, as well as mapping projects, have been done in this area by Texas A&M students. The goal of this project is to characterize the complex fault zone and to study the possibly anomalous diffusive nature of the subsurface electric currents generated by controlled source excitation.

The geology of central Texas is complex as a result of multiple tectonic events and igneous activity. A continent-continent collision created large-scale folding, faulting, and regional metamorphism in the area. Shortly after, an uplift, an igneous intrusion, and an erosional period exhumed the deeper igneous and metamorphic rocks. During the Pennsylvanian another tectonic event generated large-scale normal faults in the area. The surveyed fault is part of a graben on the edge of the Mason fault system. It is a most likely an oblique-slip fault that juxtaposes Precambrian granite and marble against Cambrian sandstone. The fault zone is characterized by numerous fractures that are parallel and orientated at an angle of 30°-60° to the slip plane. The rocks in the field site have a very low electrical conductivity which poses difficulties for the electromagnetic technique.

A loop-loop electromagnetic survey technique was used to survey the fault. A current loop (TX) acts as a magnetic dipole and the current is stepped off to induce electric eddy currents into the subsurface. The induced currents diffuse downward and outward, like smoke rings, possibly according to a vector fractional, diffusion equation. The subsurface currents generate their own weak magnetic field. The receiver (RX) is a loop and the magnetic flux through it is recorded as a function

of time after step-off of source current. The deformation and fractures in the fault zone introduce electrical anisotropy into the medium, which effects the spatiotemporal evolution of subsurface electric currents. A roughness parameter introduced into Maxwell's equations serves as a representation of the fracture density. By determination of the roughness parameter for different TX-RX offsets and orientations, this study provides insight into the structure of the fault zone.

Several electromagnetic surveys were conducted over the fault zone with acquisition geometries that included straight line, azimuthal and 3-dimensional. Finally a survey using both a source and receiver able to oriented in all three spatial directions was performed to acquire the full 9 component tensor of the electromagnetic response. The responses showed an increasing roughness with depth across the fault zone, which can be explained by deep, highly resistive features. The shallow parts of the fault showed a lower roughness value corresponding to features that are more conductive.

2. FIELD SITE AND GEOLOGY

The field site for this survey is located in Llano Uplift of central Texas, which has experienced a complex geologic history. Multiple tectonic events created fascinating geological structure, including folding, faulting, uplifting, and metamorphosed rocks. The site is the setting of numerous geological and geophysical studies.

2.1 Central Texas geology

The field site for this study is located within the Mason Mountain Wildlife Management Area (MMWMA) in central Texas. The area is approximately 6,000 acres and is owned by the state of Texas. It is located about 10 km north of the town of Mason, approximately 145 km west of Austin (Figure 2.1). Several large tectonic events created intense deformation in this area of central Texas. The Llano Orogenic Belt, which is regarded as an extension of the Grenvillian Orogeny, was created from a continent-continent collision that began between ∼1150 Ma and ∼1120 Ma and continued until ∼980 Ma (Dalziel et al. 2000). It is believed that the orogen was a collision between the Laurentian and Kalahari Cratons. Evidence for a collision comes from analysis of the geology and geochronology of the two present-day cratons. Both the Laurentian and Kalahari were active margins during the Mesoproterozoic, and the kinematics of the structures suggest a strong similarity between the two cratons (Becker 1985). Unlike the Mesozoic Andes, the presence of metamorphic rocks resulting from high pressure and temperature conditions suggest deeper burial during the collision, further indicating that the "deep-keeled" Kalahari Craton was the southern continent in the collision (Dalziel et al. 2000). Along with the regional metamorphic conditions, the collision created large folds with a northwestern-southeastern bearing (Becker 1985).

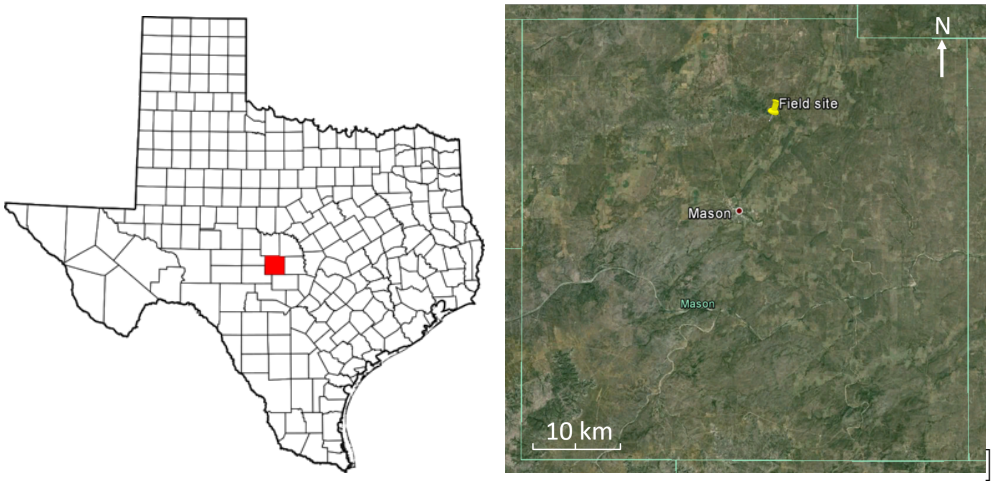

(a) (b)

(c)

Figure 2.1: a) A map of Texas with Mason county shown in red. b) Mason county and the location of the field site in relation to the town of Mason, TX. c) A close up of the field site that shows the location of the granite-sandstone fault. The granite is on the north side of the fault and the Hickory sandstone is on the the south side.

The Llano Uplift is located where the southeastern end of the Concho arch meets a northeast-southwest fault system in central Texas (Figure 2.2). A granitic pluton intruded the folded metamorphic rocks between ∼1100 Ma and ∼900 Ma. The granite formed at a depth of 6-10 km, and it was followed by 6-7 km of uplift and early Cambrian erosion (Merrill et al. 1991; Becker 1985). Today, the uplift is a gentle, square-shaped structural dome exposing metasedimentary and metavolcanic rocks created by earlier high pressure regimes (Smith & Gray 2011). The flanks of the dome are covered with Paleozoic sedimentary rocks and contain numerous faults, while the central region has no major faults (Becker 1985). The uplift covers about 3000 km^2 and is approximately centered on the town of Llano, Texas (Merrill et al. 1991). Mason county is located on the southwestern edge of the Llano Uplift, as shown in Figure 2.2.

For the Llano Uplift area, the period between the Precambrian and the Pennsylvanian was tectonically uneventful except for the occurrence of several sinks (Becker 1985). These sinks are elliptical, basin-like features that are caused by a collapse in the underlying limestone. In the early Pennsylvanian the South American plate collided with the Laurentian craton in the Ouachita orogeny. This collision created the Ouachita fold belt shown in Figure 2.2. Becker (1985) believes that lithospheric flexure and east-west extension in the Laurentian craton created numerous northeast-southwest striking, high angle normal faults parallel to Ouachita fold belt. On the other hand, Amsbury & Haenggi (1993) believe that these near vertical faults are primarily the result of north-south compression of the Llano Uplift area. From observation of outcrops in the area, they suggest that the principal movement is to the north due to a short lived compressional event in the mid-Pennsylvanian. Therefore they argue that the overall fault system possesses oblique-slip, but predominately strike-slip, motion since the outcrop patterns point more towards lateral movement

of high angle faults rather than vertical displacement along dipping faults (Amsbury 1993).

2.2 Field site

The field site is located in the Spring Pasture of the MMWMA over a northeast-southwest trending normal fault that dips at a high angle to the southeast (Figure 2.3). The pasture is used for mapping projects for Texas A&M undergraduate geology students, and it has been the site of several thesis studies for Texas A&M graduate students.

At the surface, the fault juxtaposes the Town Mountain Granite and the Hickory Sandstone (Figure 2.3). The footwall of the fault is the igneous granite and the hanging wall is the sandstone. The fault cuts across a north-south trail on the property and is visible along the road from the surface. Figure 2.4 shows the trail on the Hickory Sandstone side of the fault. The total width of the fault zone is estimated to be approximately 20 m at the point it intersects the road and the intersection is a local topographic high. On the road, and just off the road to the west, are small outcrops of the marble. Just off the road on either side is a thin layer of soil and vegetation including tall grass, Opuntia cactus and mesquite trees. The fault in this study is on the northwestern edge of the Mason fault zone, and comprises half of a horst and graben structure (Figure 2.3).

The Town Mountain Granite is a pre-Cambrian rock associated with the Llano Uplift. It is laterally extensive and outcrops in several places around the field site. The Hickory Sandstone is of middle to late Cambrian in age and is divided in three distinct subunits, upper, middle, and lower (Teran 2007). The section grades upward with finer grains in the Upper Hickory resulting from shallow marine deposition.

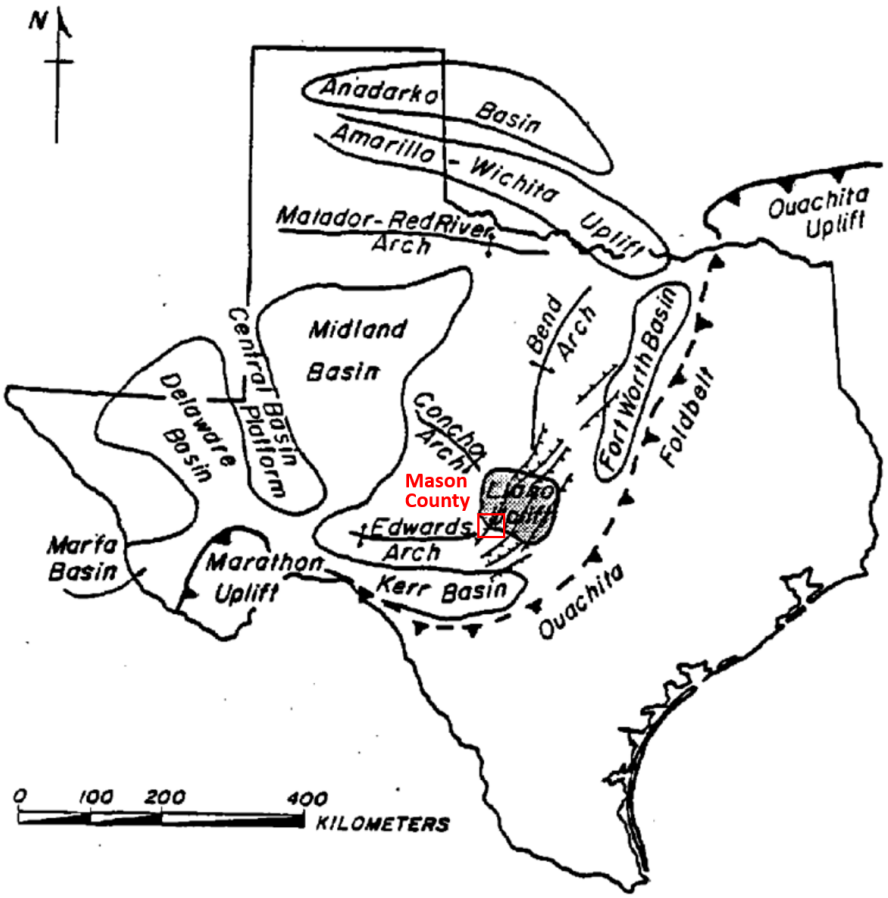

Figure 2.2: An illustration of the major tectonic events in Texas during the Carboniferous. The lines crossing the Llano Uplfit in central Texas represent normal faults that formed at the same time as the Ouachita orogeny. Mason county is located in the southwestern portion of the Llano Uplift as shown in red (Modified from Becker 1985).

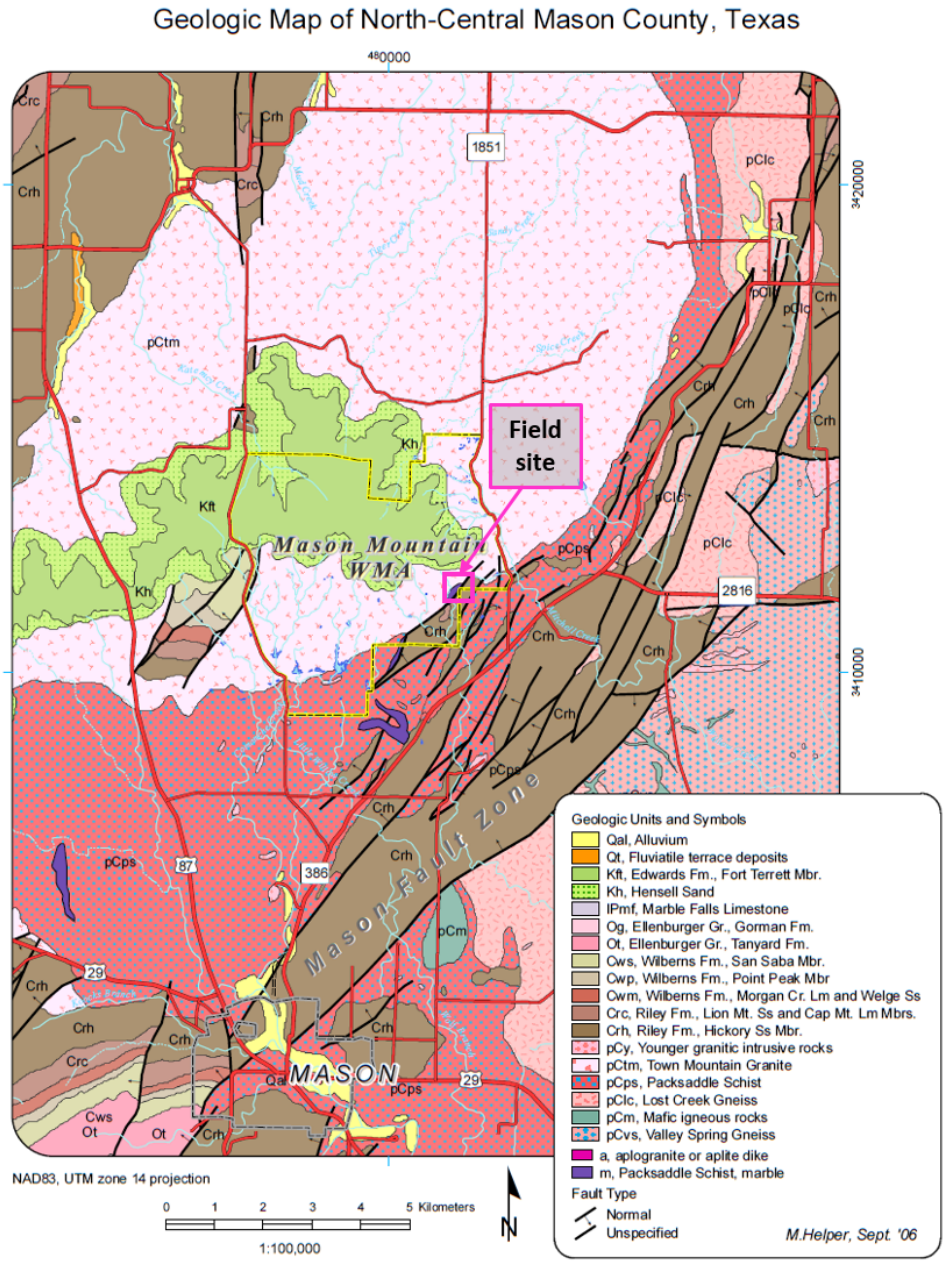

Figure 2.3: Geological map of Mason, TX and the surrounding area with the field site shown in magenta. The fault surveyed in this study is juxtaposes Town Mountain Granite with the Hickory Sandstone. In addition there is a sliver of marble on the northeast side of the fault (Modified from Helper 2006).

Figure 2.4: A picture of road that crosses over the fault, looking toward the Hickory Sandstone hanging wall.

Rock	**Conductivity** (S/m)
Dry sandstone	10^{-4} to 10^{-3}
Wet sandstone	$10^{-2.5}$ to 10^{-2}
Dry Granite	10^{-8} to 10^{-7}
Wet Granite	$10^{-4.5}$ to $10^{-3.5}$
Marble	10^{-4} to 10^{-3}

Table 2.1: A range of electrical conductivity values for the relevant rocks in the field site. The values come from different rocks with similar mineralogy to those in Mason, Texas (Gathered from Duba et al. 1978; Grandjean & Gourry 1996).

The Upper Hickory, 15 to 30 m thick, is a coarse to fine grained, well rounded sandstone that contains hematite cement and hematite ooids (Barnes & Bell 1977). The middle subunit, 55 to 70 m thick, contains fine to medium grained, well sorted sandstones and mudstones (Barnes & Bell 1977). The Middle Hickory indicates a depositional environment that was a shallow subtidal estuary along with shoreface deposits influenced by a fluvial system (Teran 2007). The Lower Hickory is more coarse grained and was deposited in a fluvial environment (Teran 2007). It is 45 to 70 m thick, coarse to medium grained, and composed of poorly sorted quartzose sandstones with mudstone intervals (Barnes & Bell 1977). The Hickory Sandstone is the lowest unit of the Riley Formation and is overlain by the Cap Mountain Limestone and the Lion Mountain Sandstone (Teran 2007). Figure 2.5 shows the relevant portion of the stratigraphic column for Mason county. The subunit at the surface of the field site is most likely the Middle Hickory Sandstone, which was determined from rock samples in the area. Table 2.1 provides typical values of the electrical conductivity of sandstones and granite samples.

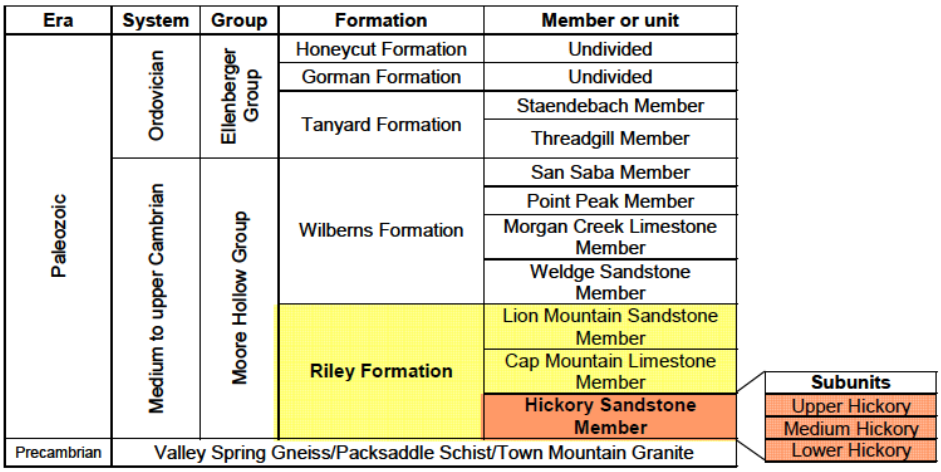

Figure 2.5: Stratigraphic column of central Texas that highlights the Hickory Sandstone of the Riley Formation. The Hickory Sandstone is the hanging wall of the fault to be studied (From Teran 2007).

2.3 Fault structure

Faults are geometrically complex structures. Those complexities reflect different phases of deformation through time, and are created by the transition of strain-hardening to strain weakening (Ben-Zion & Sammis 2003). Fault zones in brittle rocks such as both the granite and the sandstone, can be divided into two different zones (Figure 2.6). The fault core, or breccia zone, is a thin zone of highly deformed rock with cataclastic foliations and altered rocks ((3) & (4) in Figure 2.6). All of the shear displacement of the fault occurs in the fault core. The fault core is surrounded by a damage zone, or transition zone ((2) in Figure 2.6). The damage zone is much wider than the fault core and can contain fractures, microfractures, veins and mineralization (Chester et al. 2004). In most instances, the intensity of the damage zone decreases away from the fault core.

In porous, granular media, such as the Hickory Sandstone in our field site, it

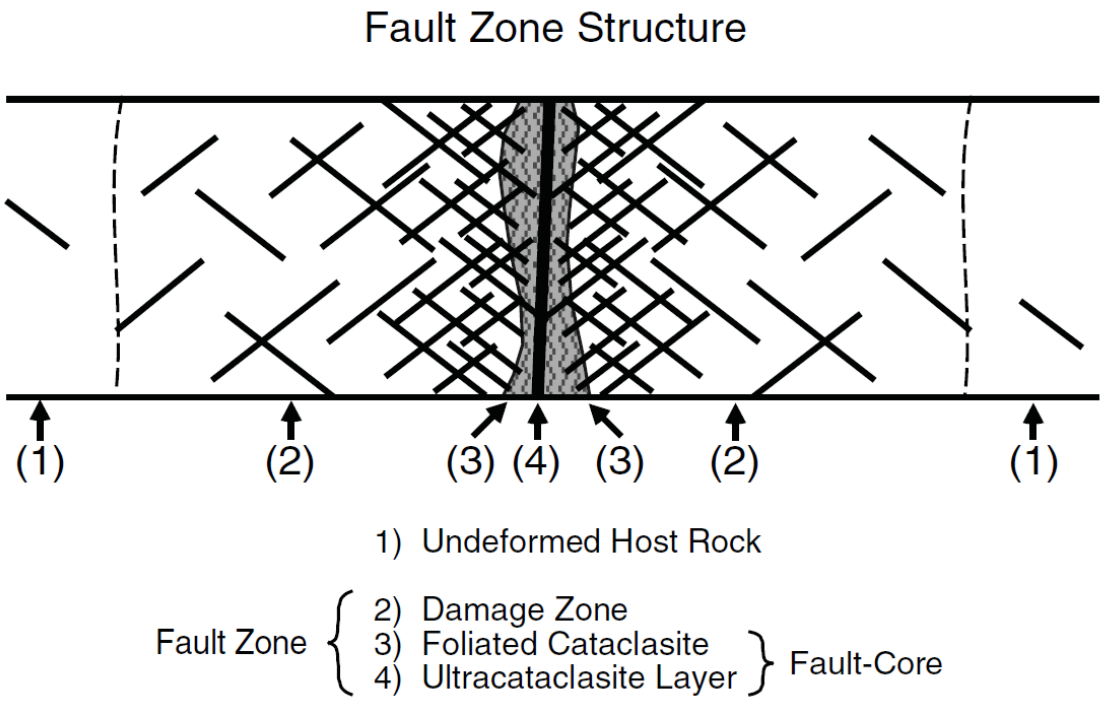

Figure 2.6: The figure is a model of fault zone structure for a brittle host rock (not to scale). The model applies to a well-lithified sedimentary or crystalline rocks. (From Chester et al. 2004)

is possible to find deformation bands (Torabi et al. 2013). Bands are found in sandstones all over the world and usually occur in rocks buried to 1.5-2.5 km, which is entirely plausible considering the geologic history of the Mason area (Fossen et al. 2007). These bands are thin planar features that are occur in the damage zone and are formed from localized stresses in the vicinity of the fault. These bands can occur in both parallel and cross-hatch patterns and they feature grain rotation, translation and cataclasis (Fossen et al. 2007). Deformation bands in the Hickory Sandstone are observed in many outcrops in the MMMWA. There can potentially be phyllosilicate smearing, dissolution, and cementation inside the bands, all of which will further reduce porosity and permeability in the band (Fossen et al. 2007). Since hydraulic and electrical pathways are highly correlated and deformation bands can negatively affect hydraulic flow, deformation bands could possibly create electrical anisotropy into the medium (Weiss & Everett 2007; Fossen et al. 2007).

Randolph (1991) studied the faults and grabens in the northern part of Mason County and how they affect the ground water system of the Hickory Sandstone aquifer, which provides valuable insight into the structure of the fault investigated in this study. The observed faults are thought to have primarily oblique-slip relative motion. The right-lateral strike-slip displacement of the faults was inferred from the overall geometry of the Mason fault zone and outcrop patterns (Randolph 1991). Due to a lack of suitable surface markers the amount of displacement can only be estimated. Using a structure map of the Town Mountain Granite and the geometries of the mapped fault system, Randolph (1991) estimates that while the magnitude of slip can vary greatly from fault to fault, the northern and southern faults are predominately dip-slip while those faults in the central area have primarily strike-slip displacement. The vertical displacement of the faults in the northern part of Mason county is less than 137 m (Randolph 1991).

Randolph's (1991) study focused primarily on the faults in the area that have Hickory Sandstone juxtaposed against Hickory Sandstone. These faults have a well-defined core, or shear zone, with a width that scales with fault displacement. There are also small faults found in close proximity to the larger faults, and they form parallel and at an angle between $30° - 60°$ to the shear zone (Randolph 1991). The core of a fault in the Hickory Sandstone is similar to others in porous quartzose sandstones in that there is a large reduction in grain size, porosity, and permeability due to cataclasis. In addition, quartz cementation, which can further reduce porosity, has been seen in localized areas along Hickory Sandstone faults. In areas along the fault where significant secondary quartz cementation occurs the core obtains characteristics of quartzite.

However, the fault in this study has Hickory Sandstone juxtaposed against the Town Mountain Granite and the metamorphic marble (Figure 2.3). The fault core will most likely feature cataclasis as in the fault in the Hickory Sandstone, but to a lesser extent. The fault zone is most likely characterized by parallel and off-angle fractures on both sides of the fault.

2.4 Previous geophysical studies

Along with several geological studies (referenced above) that were done in Mason county by Texas A&M University students, there have been a few geophysical studies conducted as well, including three projects over the studied fault. Two surveys of the fault using guided seismic waves were done along the same fault about 1 km to the southwest of the present field site (Cohrs 2012). Specifically, Cohrs (2012) conducted a seismoelectric and a seismic reflection survey along the strike of the fault, processed the data, and interpreted the results. It was observed that both methods were capable of imaging the fault by the presence of the late arriving fault

guided waves. The late arrivals were more well resolved in the seismic than the seismoelectric record as shown in Figure 2.7 (Cohrs 2012).

A magnetic survey was conducted over a 95 m $\times$ 150 m area over the same fault, just west of the trail in Figure 2.1, to image the Hickory Sandstone aquifer (Pereira 2013). The study included the acquisition of 20 lines of magnetic data in late 2012 which were then processed using reduction-to-pole filtering and Euler deconvolution among other techniques. The Euler deconvolution estimates the depth to the magnetic sources. Pereira (2013) found that the application of the Euler deconvolution resulted in a strong contrast between the magnetic data on either side of the steeply dipping fault. Figure 2.8 is a gradient map of the processed magnetic measurements with the fault interpreted (Pereira 2013).

Finally, there is an ongoing ground penetrating radar (GPR) study in the same location as this project (Amara 2015). Amara (2015) previously acquired common offset reflection GPR data over the fault, along the same line as this survey (Figure 2.9). There are a large number of point diffractions near the 80 m mark which is interpreted to be the fault zone, and the large reflections at the 120 m mark are interpreted to be the marble-granite contact (Amara 2015). Continued work by Amara (2015) will use a multi-input, multi-output (MIMO) technique to image the fault and test whether this new method increases resolution of the subsurface structure.

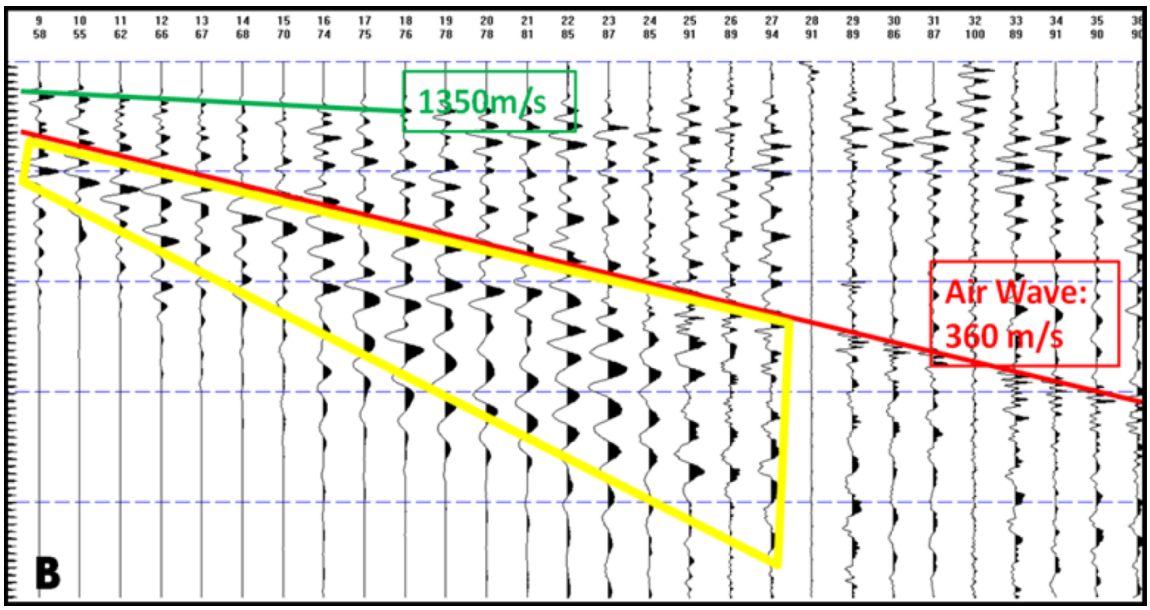

(a)

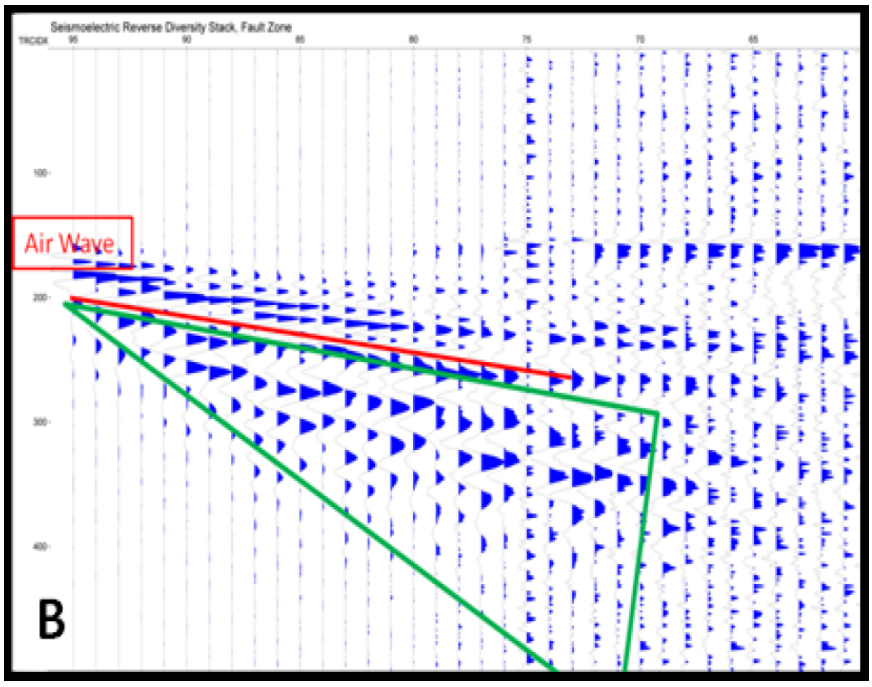

(b)

Figure 2.7: Records of the seismic (a) and seismoelectric (b) surveys along the fault zone. The red lines in each figure show the air wave and the green line in (a) shows the first motion and the P-wave velocity of the fault zone. The quadrilaterals show the late arriving fault-guided waves. (From Chors 2012).

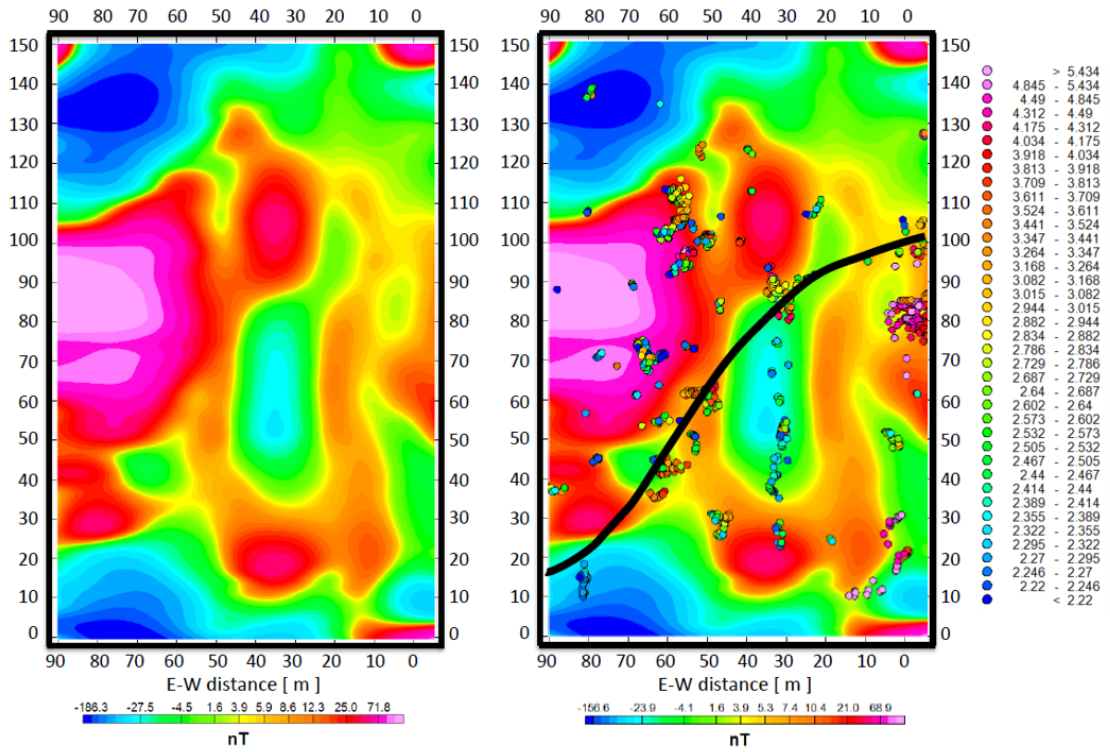

Figure 2.8: (left) A magnetic gradient map of the survey area after reduction-to-pole filtering; (right) The magnetic gradient map with Euler deconvolution overlain as well as an interpretation of the fault (From Pereira 2013).

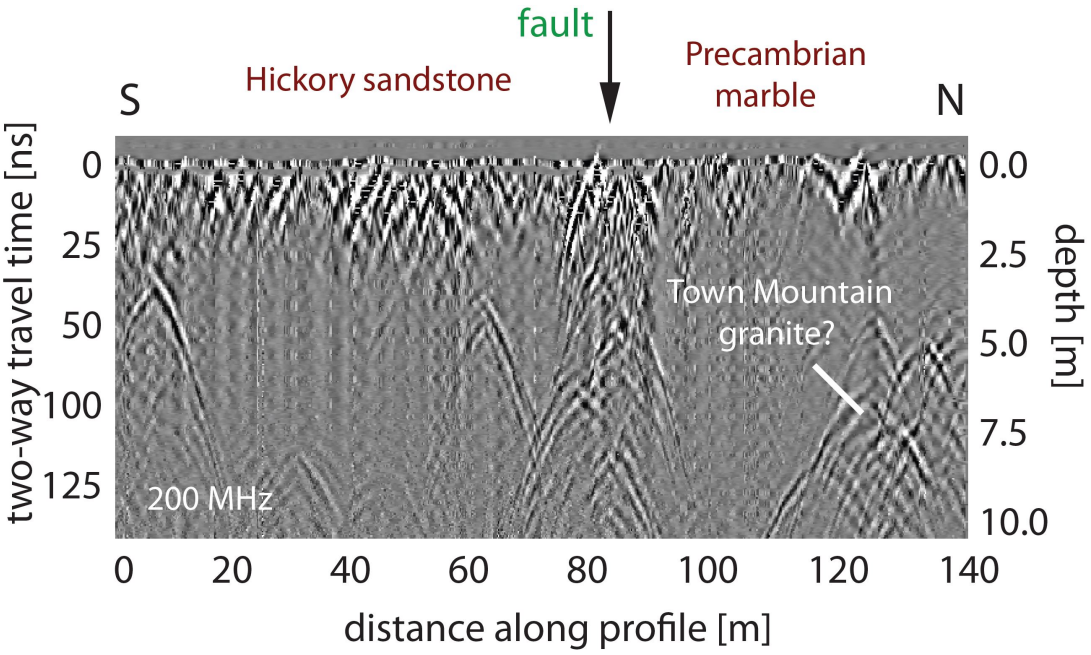

Figure 2.9: A GPR section over the fault with interpretation using the a common offset reflection technique (Amara 2015).

3. THE LOOP-LOOP ELECTROMAGNETIC METHOD

A time-domain loop-loop electromagnetic induction survey method was used for this thesis project to characterize the structure of the granite-sandstone fault. The loop-loop method has recently been used to measure subsurface electrical anisotropy in the Mason area and for studying near surface faults in the Willcox group in Texas (Collins 2004; Satti 2000).

Maxwell showed that turning on a loop source over a thin conducting sheet creates an opposing image current loop in the sheet that recedes outward at a constant velocity (Saslow 1992). However, when the conductor is a thick body, like the earth, the maximum of the induced current system moves downward as well as outward over time, like a smoke ring (Figure 3.1; Nabighian 1979). The transient magnetic field produced by the current system and measured by the receiver can be viewed as approximately due to a single ring of current in the subsurface (Nabighian 1979). The receiver measurements of the transient magnetic field are used to draw conclusions about the underlying structure of the fault.

3.1 CTRW & Anomalous diffusion

The subsurface electromagnetic eddy currents diffuse downwards and outwards into the subsurface as seen in Figure 3.1. For this project the presumption that the electric currents diffusive anomalously, which is not the conventional way interpreting electromagnetic data. One physical model for explaining the diffusion process of the electric currents begins with considering a continuous time random walk (CTRW). CTRW's provide a statistical description of problems that are generally so complex that a complete computational solution would result in far more information than is needed or desired (Giordano & Nakanishi 2006). The simplest form of a CTRW is a

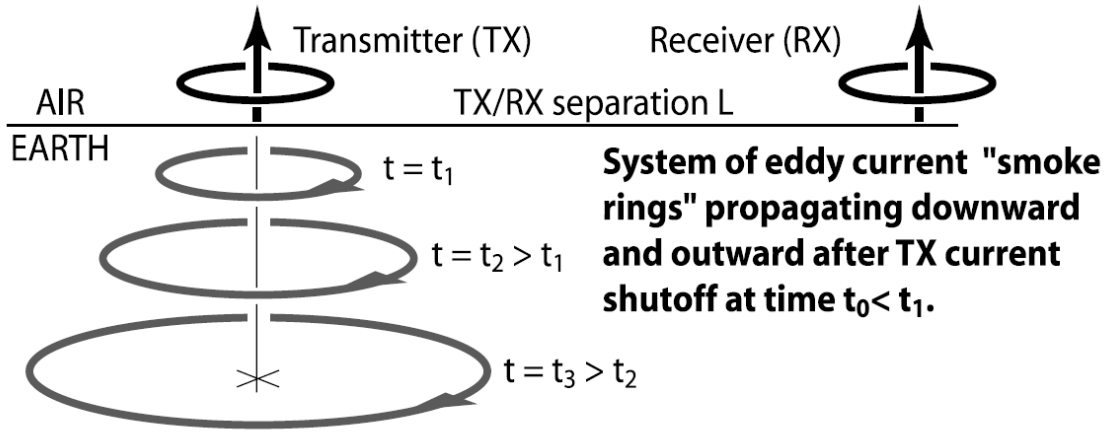

Figure 3.1: An illustration of the diffusing eddy current vortex in the theoretical half-space induced by a sharp ramp off of current in the transmitter loop (From Weiss & Everett 2007).

discrete time random walk, which for a particle in one dimension can be described mathematically by

$$x_n = \sum_{i=1}^{n} s_i \tag{3.1}$$

where n is the number of steps, x_n is the particle displacement from the origin, and s_i is a random step of unit length in either $\pm\hat{x}$ direction (Giordano & Nakanishi 2006). It can be shown that the the root-mean-square displacement from the origin of the particle,

$$\sqrt{\langle x^2 \rangle} = \sqrt{2Dt}, \tag{3.2}$$

scales as the square root of time, t (r is the displacement from the origin and D is the diffusion constant; Giordano & Nakanishi 2006). The displacement of a particle for a more generalized random walk model with steps of random length and in three dimensions also behaves according to the $t^{1/2}$ power law. For the most general case of a CTRW, the transport of particles is known as Brownian motion and is described

by,

$$B(t) = \int_{-\infty}^{t} R(s)ds, \tag{3.3}$$

where $R(s)$ contains the random variables that determine the walk of the particles with a normal distribution, a mean of zero, and a standard deviation of one (Guo et al. 2009). Brownian motion of a cluster of particles has a standard deviation of particles from the origin that is given by $\sigma_c = \sqrt{2Dt}$ (Guo et al. 2009). Particle cluster motion that scales as $t^{1/2}$ is known as classical diffusion.

A study modeling oil spill diffusion found that the particle drift does not follow normal Brownian motion (Figure 3.3). Instead the particle tracking is better described by fractional Brownian motion (fBm), where the distribution scales as $\sim t^{\alpha/2}$ (Guo et al. 2009). By studying satellite images, Guo et al. (2009) found an average value of the exponent $\alpha = 1.5$ for the particles drifting on the ocean surface. Because the observed $\alpha \neq 1$ the particle transport is said to undergo anomalous diffusion, which will be further discussed below. For this research study the induced electric currents are presumed and interpreted to diffuse according to a fBm as well.

The theory of anomalous diffusion of electric charges in semiconductors was developed from a time-dependent random walk (Scher & Montroll 1975). The function $\psi(t)$ represents the step-time distribution of the random walkers. In classical diffusion the peak and median of a propagating pulse travel at the same velocity, but in anomalous diffusion the median has a velocity that decreases with time and separates from the peak which stays closer to the origin (Figure 3.4). This is caused by a dispersion of the distances between available sites for random walkers and of the potential barriers between sites (Scher & Montroll 1975). Scher & Montroll (1975) mathematically described the difference between the two sets of curves in Figure 3.4 by the difference between the equation of the classical Gaussian propagation of the

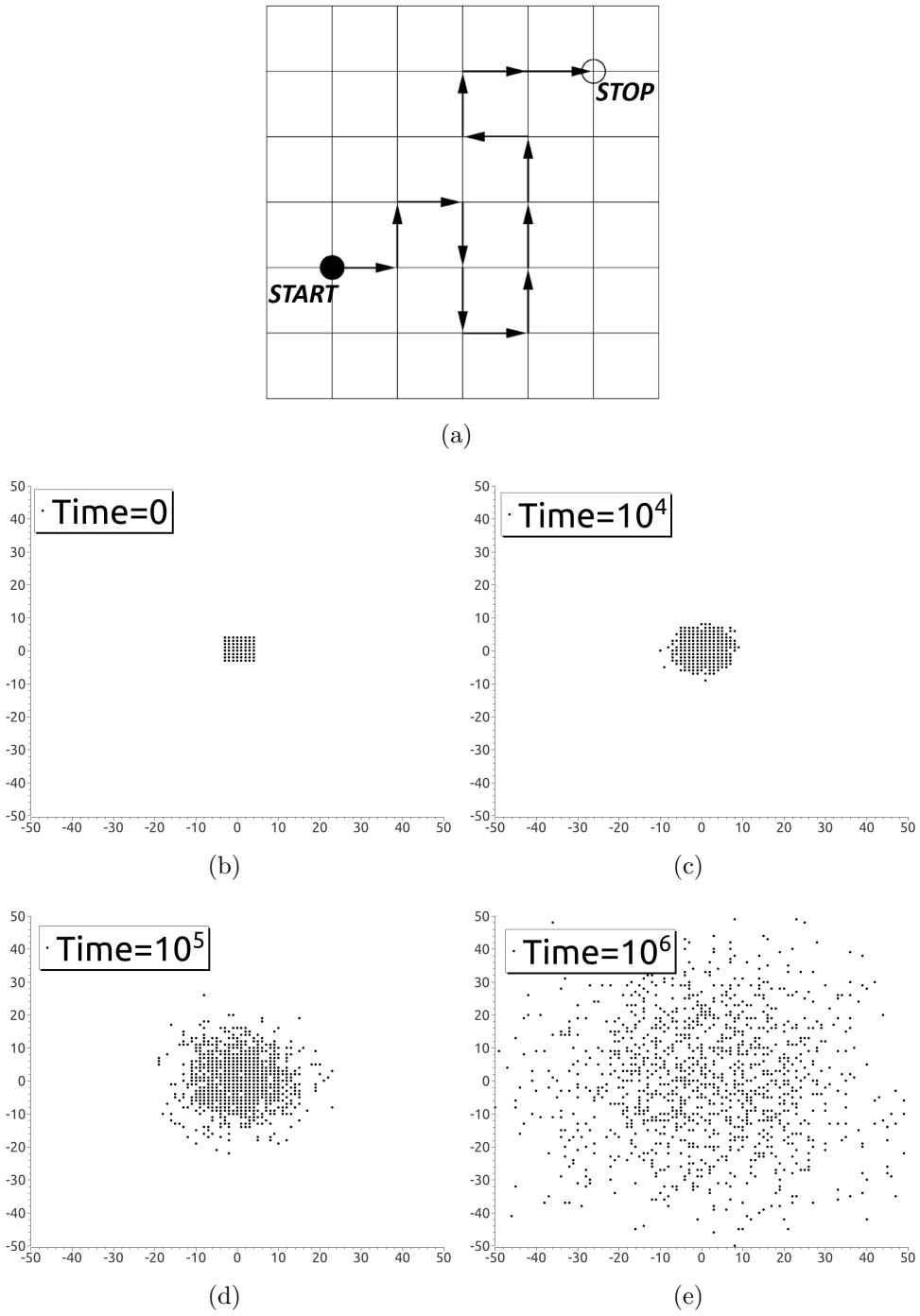

Figure 3.2: An example of a discrete time random walk on a 2D regular lattice (Modified from Metzler & Klafter 2000). (b)-(e) shows particle diffusion on a 2D lattice from normal Brownian motion at various stages after $t = 0$, a model for diffusion of a drop of cream in a cup of coffee.

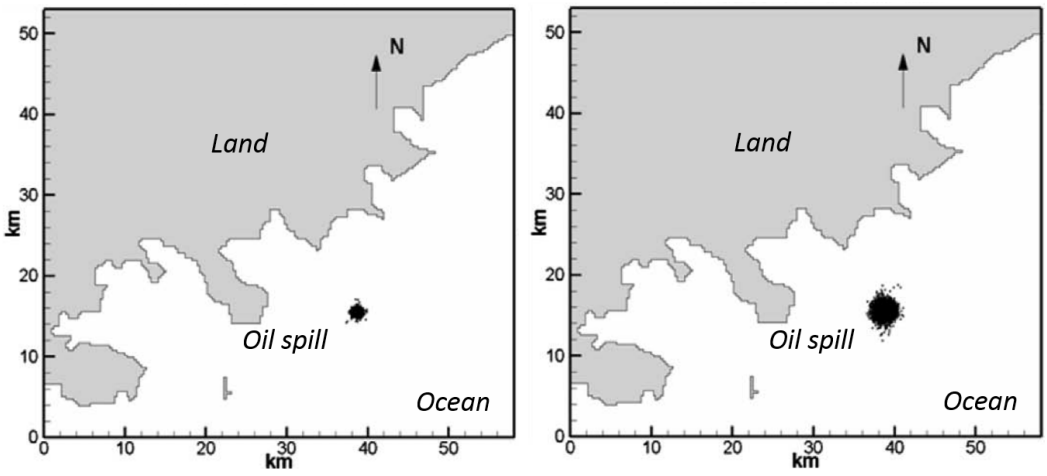

(a) (b)

Figure 3.3: (a) is a model for oil spill diffusion following a classical $t^{1/2}$ power law, and (b) is a model for oil spill diffusion following a fBm $t^{3/4}$ power law (Modified from Guo et al. 2009).

packet,

$$\psi(t) \sim e^{-\lambda t}, \tag{3.4}$$

and the anomalous diffusion of the packet

$$\psi(t) \sim \text{const} \times t^{-(1+\alpha)}, \tag{3.5}$$

where α is the anomalous diffusion exponent. While Equation 3.4 has a single transition rate, λ, Equation 3.5 is related to the distribution of a random system (Scher & Montroll 1975). The long tail of Figure 3.4 (b) can be further understood by considering that anomalous diffusion is characterized by a continuous stream of random walkers, instead of a pulse, passing through a given point for a long time (Weiss & Everett 2007).

An extensive description of anomalous diffusion can be found in Metzler & Klafter

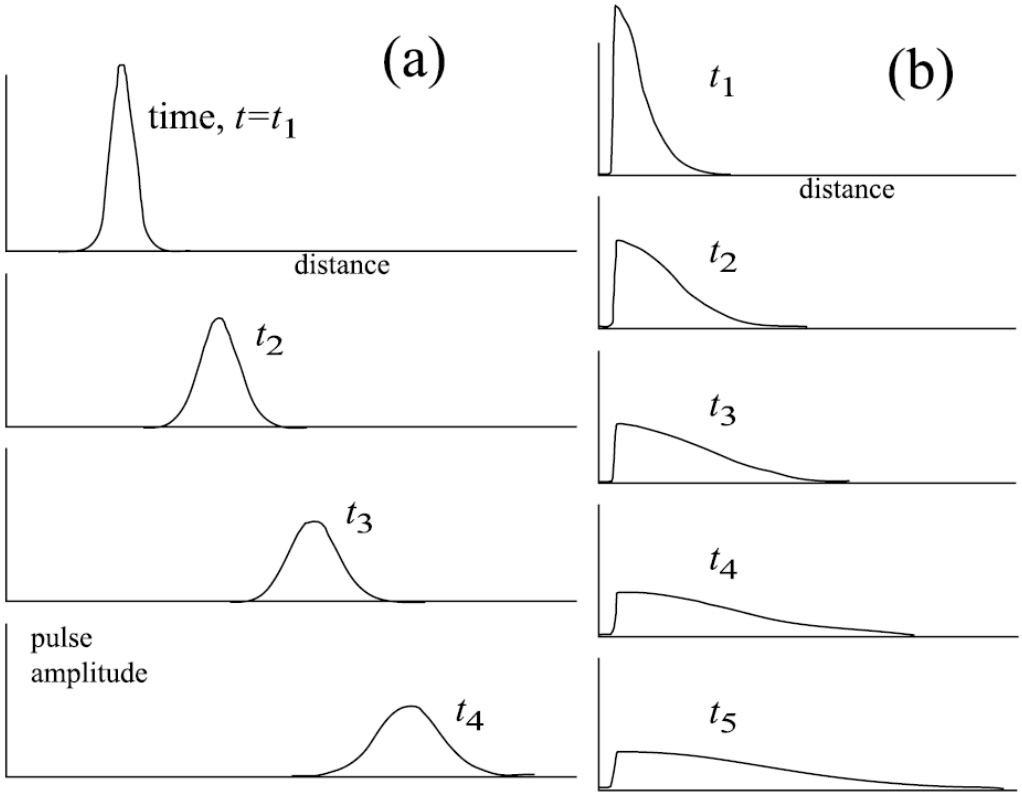

Figure 3.4: a) classical diffusion of a propagating pulse with the peak and median moving at constant velocity. b) the anomalous diffusion of the pulse with the median traveling outward from the peak with a velocity that decreases with time (From Weiss & Everett 2007).

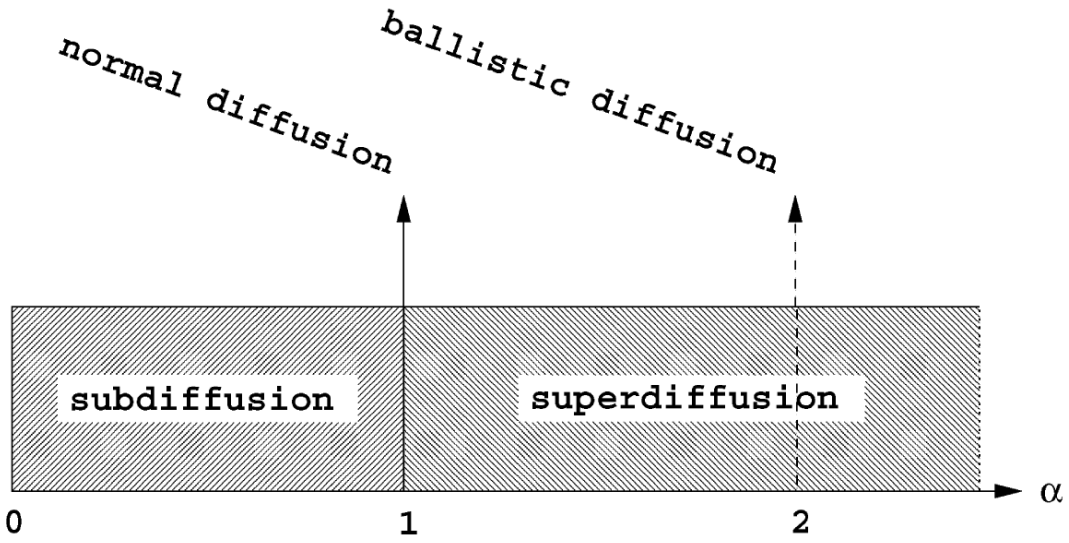

Figure 3.5: The figure shows the different domains of anomalous diffusion based on an increasing value of the diffusion constant α (From Metzler & Klafter 2000).

(2000). Figure 3.5 is an illustration of the different domains of the anomalous diffusion for different values of the anomalous diffusion exponent α. For $0 > \alpha > 1$ the anomalous transport is said to be subdiffusive. Subdiffusion is caused by some sort of feature that traps or inhibits the transport of the random walkers, and consequently the mean particle displacement is lower than for the case of classical diffusion. As alpha increases to $\alpha > 1$ the anomalous transport moves into a superdiffusive regime. Superdiffusion is caused by preferential pathways that result in a mean particle displacement that is greater than that of classical diffusion. For the special case that $\alpha = 1$, normal Brownian diffusion will occur (Metzler & Klafter 2000). There is another special case for $\alpha = 2$ termed ballistic diffusion.

3.2 Theory of electromagnetic induction

The loop-loop EM method utilizes induced current vortices to probe the electrical subsurface conductivity structure. The transmitter is a loop of finite radius that creates a magnetic field by Ampere's law,

$$\nabla \times \mathbf{B} = \mu_0 \mathbf{J}_S, \tag{3.6}$$

where $\mathbf{E}$ is the electric field, $\mathbf{B}$ is the magnetic field, μ_0 is the permeability of free space, and $\mathbf{J}_S$ is the source current density in the transmitter loop. In the fractional diffusion formulation (Weiss & Everett 2007), Ampere's law includes the generalized time-convolution of Ohm's law $\mathbf{J} = \sigma_\beta * \mathbf{E}$ (defined below in Equation 3.12) so that the previous equation becomes

$$\nabla \times \mathbf{B} = \mu_0 \sigma_\beta * \mathbf{E} + \mu_0 \mathbf{J}_S(t) \tag{3.7}$$

where σ_β is a generalized electrical conductivity and $\mathbf{J}_S(t)$ is the source current density in the loop (Everett 2009). The generalized conductivity has dimensions of $[\sigma_\beta] = \mathrm{AV}^{-1}\mathrm{m}^{-1}\mathrm{s}^{-\beta}$. The transmitter generates eddy currents in the subsurface that travel downwards and outwards with a velocity determined by the conductivity of the medium (Figure 3.1). The eddy current system is driven by an induced electromotive force (EMF) which is created by a time varying magnetic field via Faraday's law,

$$\nabla \times \mathbf{E} = -\frac{\partial \mathbf{B}}{\partial t}. \tag{3.8}$$

The induced eddy currents obey Lenz's law, which dictates the direction of the induced current flow. For induction in the subsurface the EMF in a closed path is

given by $\mathcal{E} = -\frac{\partial \Phi}{\partial t}$, where Φ is the magnetic flux through the loop. The negative sign in the induced EMF is the mathematical representation of Lenz's law, and is present because a conducting loop, or medium, prefers to maintain a constant flux through it (Griffiths 1999). If a change in the flux occurs then a current will be produced in the direction so as to counteract the change in flux (Griffiths 1999). This is equivalent to the conservation of energy.

The current in the source loop, I_S which is user-controlled in the field, quickly drops from a designated amperage to zero. The step-off is actually a linear ramp-off to avoid oscillatory transients. The magnetic field produced by the source loop then decreases as a function of time, and the subsurface currents are generated. The subsurface currents produce their own magnetic fields, also by Ampere's law (Equation 3.6). Finally, the magnetic flux through the receiver loop is recorded as a function of time after the source current ramp-off.

Previous work (Weiss & Everett 2007) suggested that controlled source electromagnetic induction in a spatially hierarchical heterogeneous medium may behave as an anomalous diffusion process and can be described by a fractional diffusion equation. The general time-fractional diffusion equation can be written as

$$\frac{\partial}{\partial t} A(x,t) = {}_0D_t^{1-\alpha} \left[v_\alpha \frac{\partial^2}{\partial x^2} A(x,t) \right] \tag{3.9}$$

where the differentiation operator ${}_0D_t^{1-\alpha}$ is

$${}_0D_t^{1-\alpha} A(x,t) = \frac{1}{\Gamma(t)} \frac{\partial}{\partial t} \left[\int_0^t \frac{A(x,t')}{(t-t')^{1-\alpha}} dt' \right] \tag{3.10}$$

and v_α is the generalized diffusion constant. Equation (3.9) mathematically describes the process of anomalous diffusion and reverts to the classical diffusion equation,

when $\alpha \to 1$ (Weiss & Everett 2007).

Combining equations (3.7) and (3.8) leads to

$$\nabla \times \nabla \times \mathbf{E} = -\mu_0 \frac{\partial}{\partial t}[\sigma_\beta * \mathbf{E} + \mathbf{J}_S] \tag{3.11}$$

which is a vector diffusion equation for the electric field (Everett 2009). Weiss & Everett (2007) showed the equation for the anomalous diffusion of the electric field $\mathbf{E}$ can be represented by a fractional diffusion equation achieved by using the aforementioned generalized form of Ohm's law so that

$$\sigma \mathbf{E} \to \sigma_\beta * \mathbf{E} \equiv \int_0^t \frac{\mathrm{d}t' \sigma_\beta \mathbf{E}(t')}{(t-t')^{1-\beta}} \tag{3.12}$$

and the authors refer to σ_β as the "anomalous electrical conductivity." The new parameter β is referred to as the "roughness parameter" by Weiss & Everett (2007), and it presumably serves as a proxy for the fracture density of the medium (Decker & Everett 2009). Taking the roughness parameter to be infinitely small, $\beta \to 0$, would correspond to a smooth continuously differentiable geologic medium.

The time derivative of equation (3.12) is

$$\frac{\partial}{\partial t}\sigma_\beta * \mathbf{E} = \frac{\sigma_\beta}{\Gamma(\beta)} \frac{\partial}{\partial t} \int_0^t \frac{\mathbf{E}(t')\mathrm{d}t'}{(t-t')^{1-\beta}} \equiv \sigma_\beta \, {}_0D_t^{1-\beta} \mathbf{E}(t) \tag{3.13}$$

where the Γ function serves as a normalizing constant (Everett 2009). Combining equations (3.13) and (3.11) results in

$$\nabla \times \nabla \times \mathbf{E} = -\mu_0 \sigma_\beta \, {}_0D_t^{1-\beta} \mathbf{E}(t) - \mu_0 \frac{\partial}{\partial t} \mathbf{J}_S \tag{3.14}$$

which is the equation governing EM induction in a rough geological medium (Everett

2009). In the case that $\beta \to 0$, equation (3.14) reverts to the classical vector diffusion equation,

$$\nabla \times \nabla \times \mathbf{E} = -\mu_0 \frac{\partial}{\partial t}[\sigma \mathbf{E} + \mathbf{J}_S]. \tag{3.15}$$

The fractional diffusion equation, Equation 3.14, can be easily solved in the Laplace s-domain by taking the Laplace transform $L\{\}$ resulting in

$$\nabla \times \nabla \times \mathbf{e}(s) = -\mu_0 \sigma_0 s^{1-\beta} \mathbf{e}(s) - \mu_0 s \mathbf{j}_s(s) \tag{3.16}$$

where $\mathbf{e}(s)$ and $\mathbf{j}_s(s)$ are the Laplace-transformed electric field $\mathbf{E}(t)$ and source current density $\mathbf{J}_s(s)$ respectively (Everett 2009).

The following derivation will consider the case of a horizontal source current loop above a uniform half-space. Since the electric field is axisymmetric, Equation 3.16 can be solved in cylindrical coordinates and can be found by taking a Hankel transform and utilizing the boundary conditions at the air-earth interface. In the subsurface the eddy currents are generated by the step-off of the source current, but it is more convenient, at first, to determine the step-on response. The step-on electric field in the subsurface is given by

$$e_\phi^{STEP-ON}(s) = -\frac{\mu_0 I a}{2} \int_0^\infty \{exp[-\lambda(z+h)] + Rexp[\lambda(z-h)]\} \times \mathrm{J}_1(\lambda a)\mathrm{J}_1(\lambda \rho)\mathrm{d}\lambda, \tag{3.17}$$

where z is depth, h is the height of the source loop above $z = 0$, and J_1 is the 1^{st} order Bessel function (Everett 2009). The circulating electric field, $e_\phi^{STEP-ON}(s)$, is proportional to the eddy current density (Everett 2009). In practice, the receiver measures the time-derivative of the vertical magnetic field produced by the eddy currents, which can be found by applying Faraday's law (Equation 3.8) to Equation

3.17,

$$h_z^{STEP-ON}(s) = \frac{Ia}{s}\int_0^\infty \frac{\lambda^2}{\lambda+\gamma}\mathrm{J}_1(\lambda a)\mathrm{J}_0(\lambda\rho)\mathrm{d}\lambda. \tag{3.18}$$

for the case that $h = 0$ and $z = 0$ (Everett 2009). The step-off magnetic field measured by the receiver is then determined by

$$h_z^{STEP-OFF}(s) = h_z^{DC} - h_z^{STEP-ON}(s) \tag{3.19}$$

where h_z^{DC} is the late-time response (Everett 2009). A detailed derivation of the transient response of a finite-sized loop above a homogeneous or layered half-space can also be found in Ward and Hohmann (1987).

3.3 Effect of anisotropy

The horizontal loop-loop electromagnetic survey method is ideal for detecting horizontal anisotropy, such as in the model in Figure 3.6 (Everett 2006). The model shows parallel vertical sheets, meant to represent fractures, of material embedded in a background medium. Because the conductivity of the sheets differs from the background conductivity, the medium is electrically anisotropic, meaning the apparent conductivity, σ_a, is different in different directions. For the model in Figure 3.6, the conductivity in the direction perpendicular to the sheets, $\sigma_\perp$, is less than the conductivity along the strike of the sheets, $\sigma_\#$.

For loop-loop surveys σ_a observed in a given direction will be equal to the geometric mean of the electrical conductivities in the other two orthogonal directions (Everett 2006). In this way the the apparent conductivity is greater across the strike of the sheets than parallel to the sheets. This electromagnetic anisotropy paradox for loop-loop surveys illustrated by the right of Figure 3.6. For a real-world geology

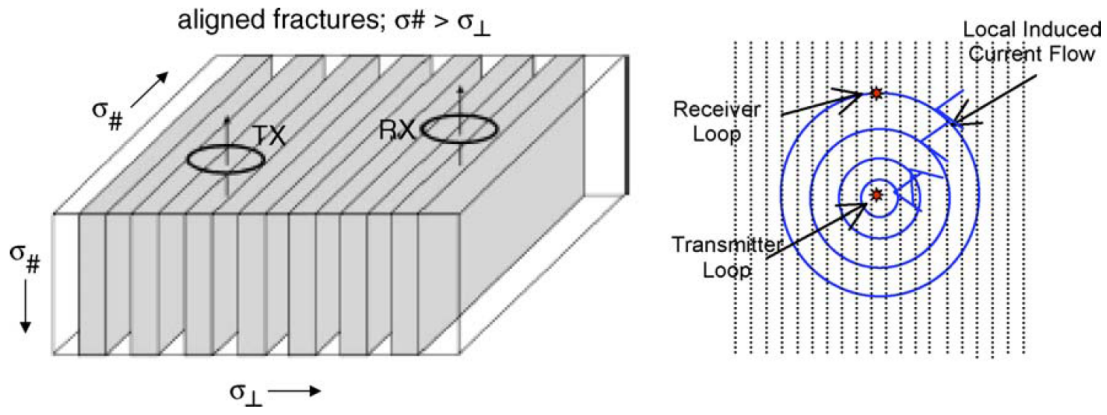

Figure 3.6: The left figure is a model of a vertically fractured geology with anisotropic electrical conductivity. The figure on the right is top-down view of the model and illustrates the electromagnetic anisotropy paradox. Both are further explained in the text (From Everett 2006).

the anisotropy can described by the tensor

$$\begin{pmatrix} \sigma_{xx} & \sigma_{xy} & \sigma_{xz} \\ \sigma_{yx} & \sigma_{yy} & \sigma_{yz} \\ \sigma_{zx} & \sigma_{zy} & \sigma_{zz} \end{pmatrix}. \tag{3.20}$$

Several geological factors can create electrical anisotropies in the subsurface including bedding planes, fractures, and foliations (Collins 2004). For the field site in this study the most likely causes of anisotropy in the subsurface are the fractures and potentially deformation bands in the damage zone, as well as the fault core. The fractures in the fault zone will be both parallel and intersecting and will be of varying length scales. Conductivity anisotropies in the subsurface can effect the diffusive behavior of the eddy currents.

4. DATA ACQUISITION

Several field trips were made to the MMWMA in order to acquire the time-domain electromagnetic data sets. The surveys were conducted over the field site starting in the Spring of 2012, and ultimately finishing with a survey in February 2014. Data were acquired with the assistance of several other students and the committee chair.

4.1 EM equipment

A Geonics TEM47 transmitter and Geonics PROTEM 3-component receiver were used to acquire the data over the fault. The electromagnetic surveying equipment is on loan to Texas A&M University's Department of Geology and Geophysics from Virginia Tech University.

The Geonics TEM47 transmitter is a small and light battery powered device that is specifically designed to for the measurement of the near-surface electromagnetic response. The transmitter outputs a rectangular waveform to the source loop and has base frequencies of 30, 75, or 285 Hz. The turn off-time, which induces the electric currents, is variable and can be controlled on the system, but the shortest ramp-off time is 0.5μs. The current in the source loop also can be controlled, however the transmitter used in this study produced a current that was somewhat unsteady over time. For the 2012 surveys the source loop was a single wire loop with a radius of approximately 5 m that was laid on the ground. In order to acquire the full 9 component tensor of EM data, a new source was used that could be oriented in the x, y, and z directions (Figure 4.1).

The Geonics PROTEM receiver used in this study records the rate of decay of the magnetic flux through the receiver coil in nV/m^2. It takes measurements at either 20 or 30 logarithmically spaced time gates from either 6.8 μs to 695 μs or

Figure 4.1: The 3-D source used for data acquisition in Mason, TX. The wire loop used to create the magnetic field is threaded through the circular PVC pipe. The loop can be rested on the top of the stand (as shown above) for either the x or y orientations, or it can be suspended from the top of the stand in a horizontal position for the z orientation.

6.8 μs to 6978 μs respectively. The receiver utilizes integration times from 0.5 s up to 120 s in order to average several response curves to reduce noise. The receiver is connected to the transmitter via a reference cable, which allows the receiver to know precisely when the transmitter ramp-off occurs. For this study a 3 component receiver coil (Figure 4.2) was used to measure the x, y, and z components of the magnetic field. The PROTEM receiver can use a single channel to measure one component or sequentially measure all 3 components, or use 3 channels to measure 3 components simultaneously.

4.2 Previous surveys

The student acquired data from several surveys at this field site over a time period of 2 years, but after analysis of the data set it was determined that the signal to noise ratio (SNR) was too low to be effectively analyzed. The first survey was in the spring of 2012 as undergraduate research. The equipment used for this field trip was the TEM47 owned by Texas A&M University. The source used was the 5 m radius wire loop and the receiver was a single coil that measured only in the magnetic field in the z direction. A straight line survey was completed with the source loop placed on the sandstone hangingwall and receiver locations stepping out every 2 m northward across the fault to a final TX-RX offset of 150 m. Another straight line survey was conducted with the source on the granite footwall and receiver locations similarly stepping out to the south. In addition, an azimuthal survey was conducted with the source loop close to the fault and receiver locations with 5 m spacings along a circular arc with a radius of 50 m. Because of limitations in the field, i.e. brush and cacti, we were unable to complete a full circle for this survey, but the receiver locations did cross over the fault in two locations. Finally in the Spring of 2013, much work was done trying to acquire a 3 dimensional data set over an area of

Figure 4.2: The receiver coil used in this study is shown. There are 3 separate coils in order to measure the x, y, and z components of the magnetic field produced by the subsurface currents.

approximately 150 m by 150 m. There were 5 transmitter locations each with about 25 randomly selected receiver locations each. The 3 component receiver was used to measure each component of the magnetic field. In order to determine the locations of the transmitter and receiver sites a total station was used to find distances and angles from reference points in the area. The purpose of the 3-dimensional survey was to rigorously test if the electric currents diffused anomalously in the subsurface. A schematic of these surveys can be seen in Figure 4.3.

After a thorough examination of the 2012 survey data it was determined there was a large amount of noise in each data set. A short integration time was used in an effort to increase the speed of acquisition. In addition, inspection of the 3-D data set indicated the 3 component pre-amplifier connecting the receiver coil to the PROTEM receiver was not working properly. The acquisition methodology was altered in order to overcome these issues and is described in detail in section 4.3.

4.3 Acquisition methodology

The full 9 component EM tensor data set was acquired over the field site in February 2014. With the 3 component source and the 3 component receiver (Figure 4.4) it is possible to acquire all 9 components of the tensor,

$$\frac{\partial}{\partial t}\begin{pmatrix} B_{xx} & B_{xy} & B_{xz} \\ B_{yx} & B_{yy} & B_{yz} \\ B_{zx} & B_{zy} & B_{zz} \end{pmatrix} \tag{4.1}$$

where $\frac{\partial}{\partial t}B_{ij}$ is the response measured with the source in the i orientation and the receiver oriented in the j direction, as a function of time after transmitter ramp-off. Two surveys were completed at the field site. For survey 1 the source is located on the granite footwall (north side of the fault) with receiver locations stepping

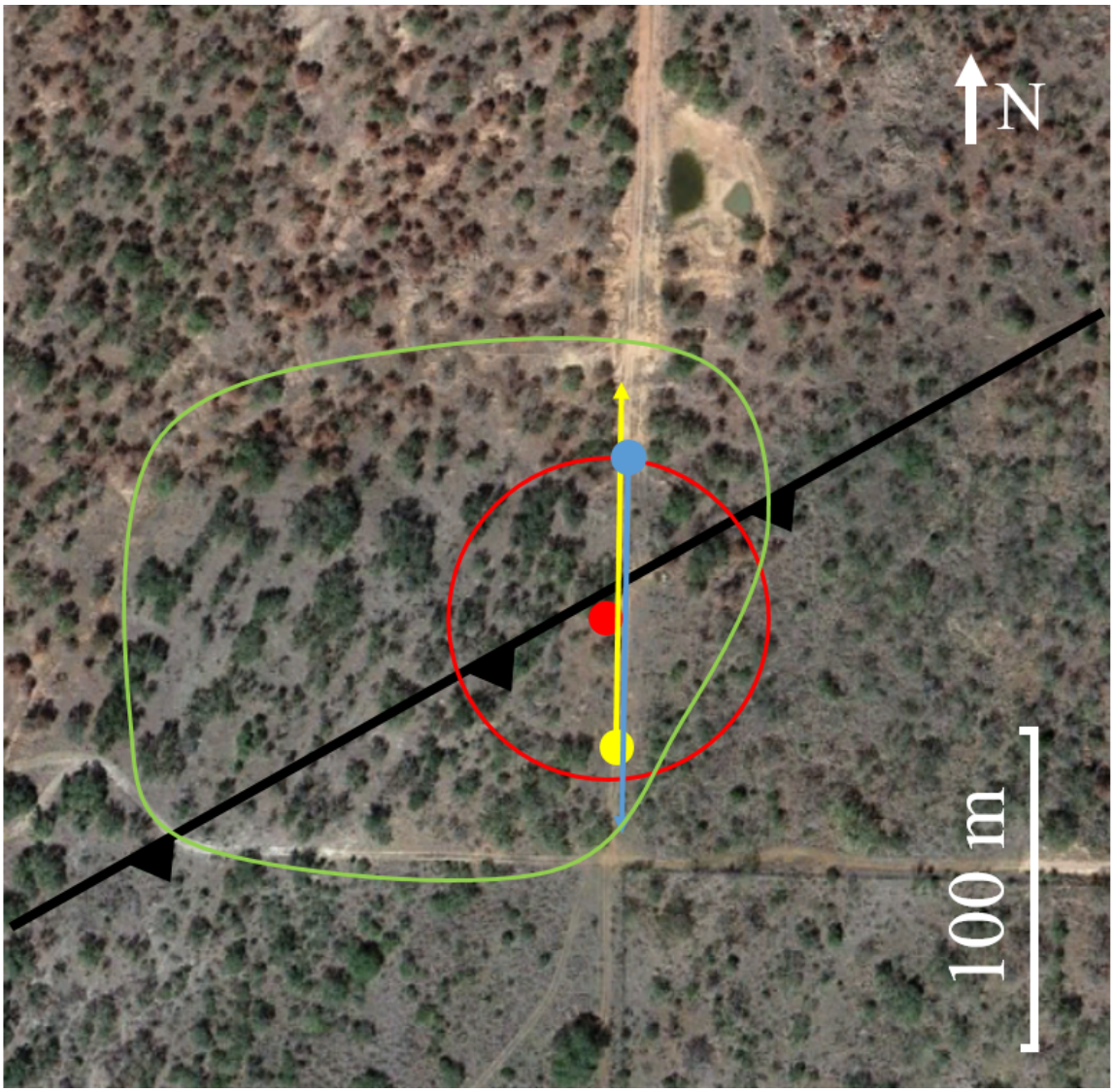

Figure 4.3: A map of the field site and a depiction of the 2012 surveys. The straight-line surveys in both directions over the fault are depicted in blue and yellow where the source is a circle and receiver locations follow the line extending from them. The small filled red circle and larger red circle represent the source and receiver locations of the radial survey respectively. The green area represents the coverage of the 3-D survey.

(a) (b)

Figure 4.4: (a) is a picture taken at the field site of the Geonics receiver coil on the granite (northern) side of the fault, and (b) is a picture of the new transmitter loop setup shown in laying on the ground in the z -configuration connected to the TEM47 transmitter. The receiver features three coils for the x, y and z components of the magnetic field. The receiver is connect to a pre-amplifier which is connected to the PROTEM receiver for data collection. The transmitter coil is wrapped in a loop of PVC pipe and can be oriented in the x, y or z directions.

out south across the fault. The source for survey 2 is on the sandstone hanging wall (south side of the fault) with receiver locations stepping out north across the fault. In order to increase the SNR an integration time of 120 s was used. In addition, because the z channel of the pre-amplifier was the only one thought to be working properly, the measurements must be taken one component at a time and the connections between the pre-amplifier and the receiver coil must be switched between each measurement. These factors greatly increased the acquisition time from previous surveys, and therefore it was only possible to acquire a few TX and RX stations over the fault. Ultimately due to the limited amount of time available, 8 receiver locations were completed for both surveys. These receiver locations ranged from 15 m to 50 m TX-RX offset at 5 m intervals. A schematic of the survey geometry can be seen in Figure 4.5.

There were two main issues that caused problems during acquisition of the EM data. The transmitter only had one functioning battery, and the increased acquisition time meant that the battery had to be recharged during the day. In addition, the current output from the transmitter was erratic at times (Figure 4.6). The current is important to know because it is used to normalize all of the EM responses to 1.0 A. The transmitter current was checked with every change of the source orientation and interpolated for measurements at times in between. It is possible that the current fluctuated between checks and could be significantly different than what was recorded. Variations in the current would not alter the magnitude of the late time slope, discussed in the following section, after normalization, but it would alter the magnitude of the response.

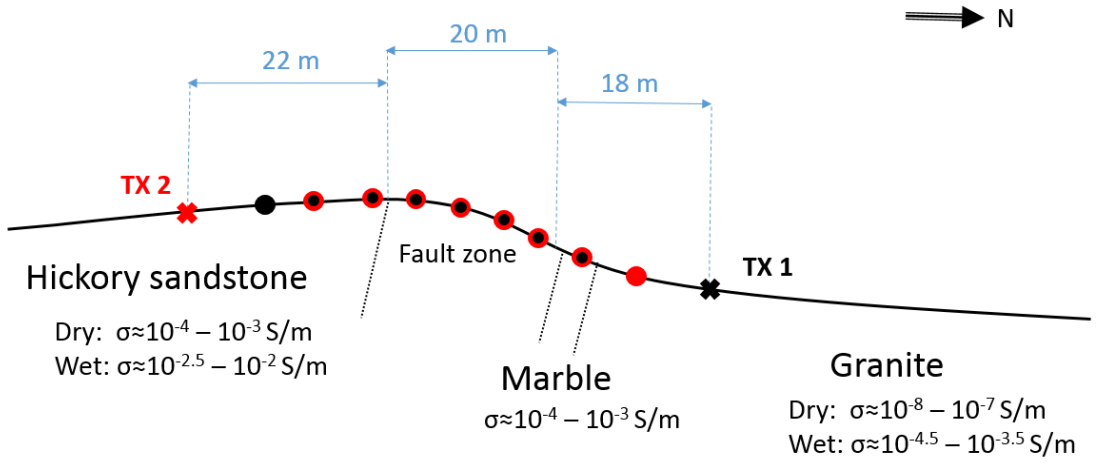

Figure 4.5: The figure is an illustration of the acquisition geometry for the 9 component tensor survey (not to scale). The source for survey 1 in was on the granite footwall and the source for survey 2 was on the sandstone hanging wall. The fault zone is approximately 20 m wide at the location of the surveys. The black and red circles show receiver locations red circles represent receiver locations for each respective survey. The total relief is on the order of a few meters.

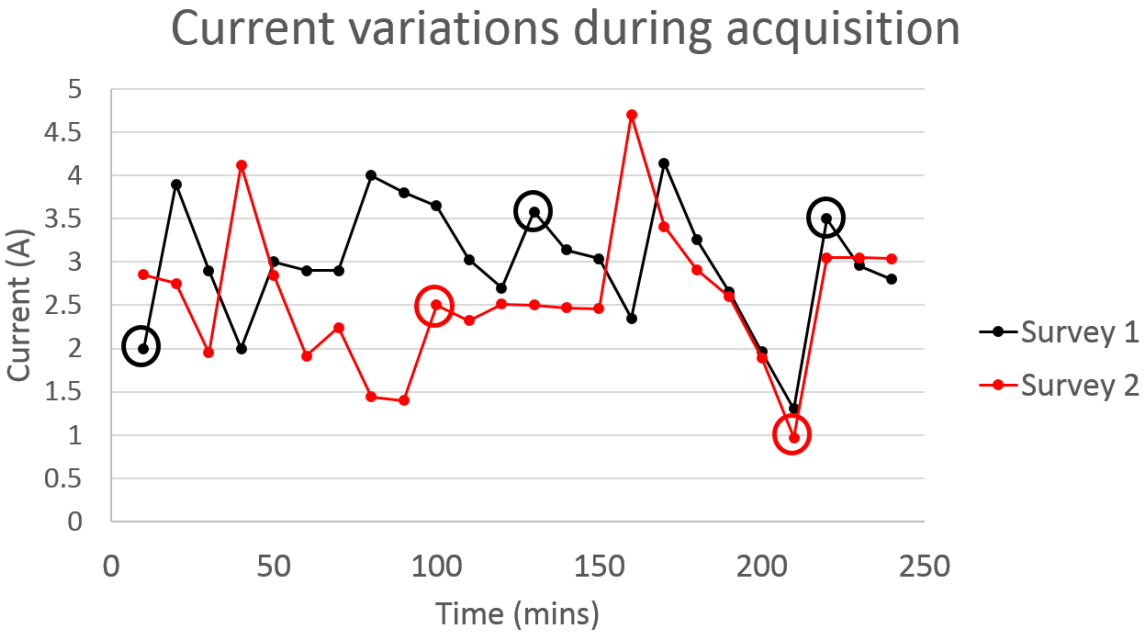

Figure 4.6: A plot of source current for surveys 1 and 2. Readings were taken during change of source orientations every 3 measurements, approximately every 10-15 mins. The circled points indicate when the battery was fully charged.

5. EM DATA ANALYSIS AND INTERPRETATION

The loop-loop electromagnetic induction method is especially useful for examining horizontal anisotropy in the subsurface (Everett 2006). The fault effectively introduces complex anisotropic structure into the conducting geological medium due to the network of fractures in the fault zone. By analyzing and interpreting the acquired data set presuming that the electric currents diffuse anomalously, inferences about the structure of the fault at depth can be made.

5.1 Data analysis

Theoretically the classical step-off transient response for the acquired data set will look similar to the dashed line in Figure 5.1. The cusp in the dashed line corresponds to the zero-crossing time of the magnetic field measured by the receiver. This is the time after step-off at which the radius of the subsurface eddy current is approximately equal to the TX-RX offset. At the zero-crossing time the magnetic flux through the receiver loop changes direction. The classical late-time decay has a linear slope of $-5/2$. Previous studies in conductive environments (Figure 5.3) show EM responses to have the familiar shape of the dashed line.

The subsurface of the filed site in Mason,TX has a much higher resistivity than those in Figure 5.3 as well as multi-scale heterogeneity. In a homogeneous half space the downward velocity and the radius of the eddy currents is given by

$$v = 2/(\pi\sigma\mu_0 t)^{1/2} \tag{5.1}$$

and

$$r = ((4.37t)/\sigma\mu_0)^{1/2} \tag{5.2}$$

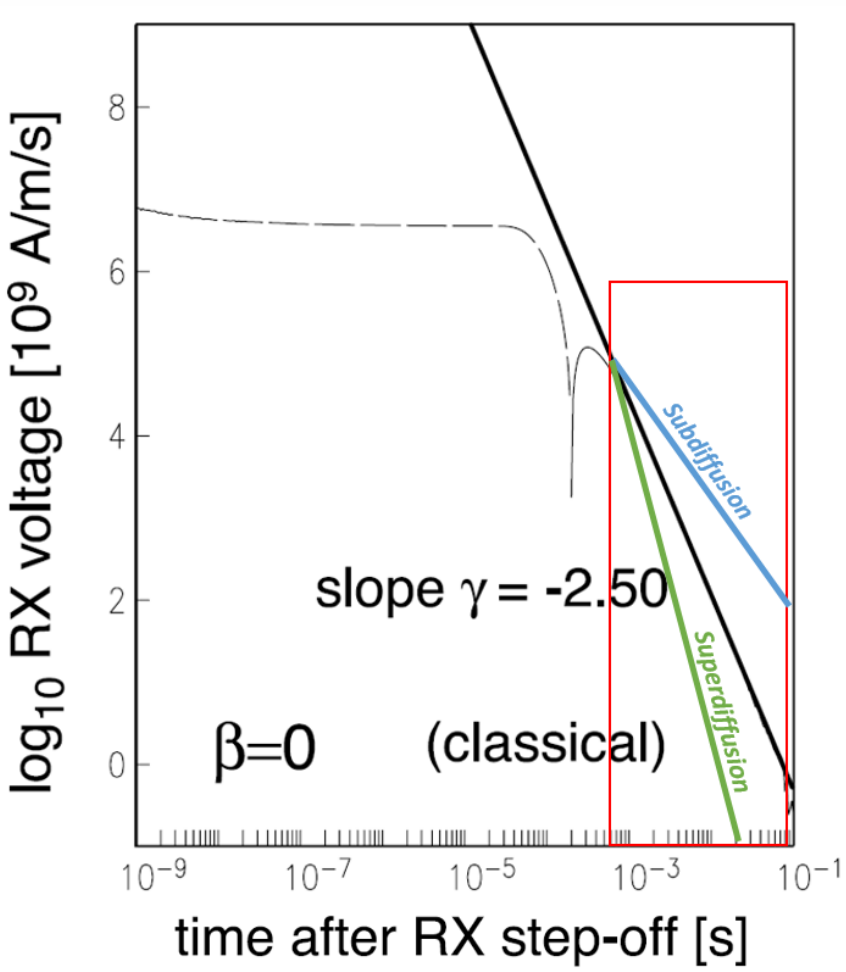

Figure 5.1: The figure shows a theoretical log-log plot of the EM response as a function of time. The dashed line is the response and the solid line depicts the late time slope. The late time slope is -2.50 which is representative of classical diffusion. If the late time slope is shallower than -2.50 then the medium is subdiffusive, and if the slope is steeper than -2.50 then the medium is superdiffusive. The red box represents the decay of the EM response, which is what was recorded in Mason, TX (Modified from Everett 2009).

respectively, where σ is the conductivity of the lower half-space (Nabighian 1979). Because of the inverse relationship between conductivity and the velocity and radius of the subsurface electric current, the more resistive the subsurface the faster the move out of the induced electric current will occur. Figure 5.2 shows the logarithmic value of the response of the z-directed TX loop and z-directed RX loop at various offsets for both surveys. After inspection of the acquired data set it is believed that the data only represents the portion of the response curve after the cusp as shown by the red window in Figure 5.1. For all offsets the zero-crossing time would most likely occur before the first time gate of 6.8 μs, so the zero crossing time is not recorded for any location in either survey. The recorded data only show the relatively late-time decay of the EM response.

The bold line in Figure 5.1 is a line tangent to the dashed curve representing the late-time slope of the TEM47 response. For the case of a homogeneous half space, the time derivative of the magnetic field decays as

$$\frac{\partial h_z}{\partial t} \approx \frac{I(\sigma\mu_0)^{3/2}a^2}{20\pi^{1/2}}t^{-5/2} \tag{5.3}$$

(Ward & Hohmann 1987). The late-time slope, the bold line, in Figure 5.1 shows the classical decay of $\gamma = -5/2$. EM responses that decay slower, meaning a late-time slope $\gamma > -5/2$, are said to undergo sub-diffusion. EM responses with a steeper decay, a late-time slope $\gamma < -5/2$, decay faster and undergo super-diffusion. Most of the EM data acquired in Mason, TX has a $\gamma < -5/2$ indicating a super-diffusive propagation of eddy currents in the subsurface.

Upon further inspection of the data acquired in Mason, TX, it was determined that the late-time slope is best estimated by the first 10 time gates, 6.8 μs to 70.3 μs.

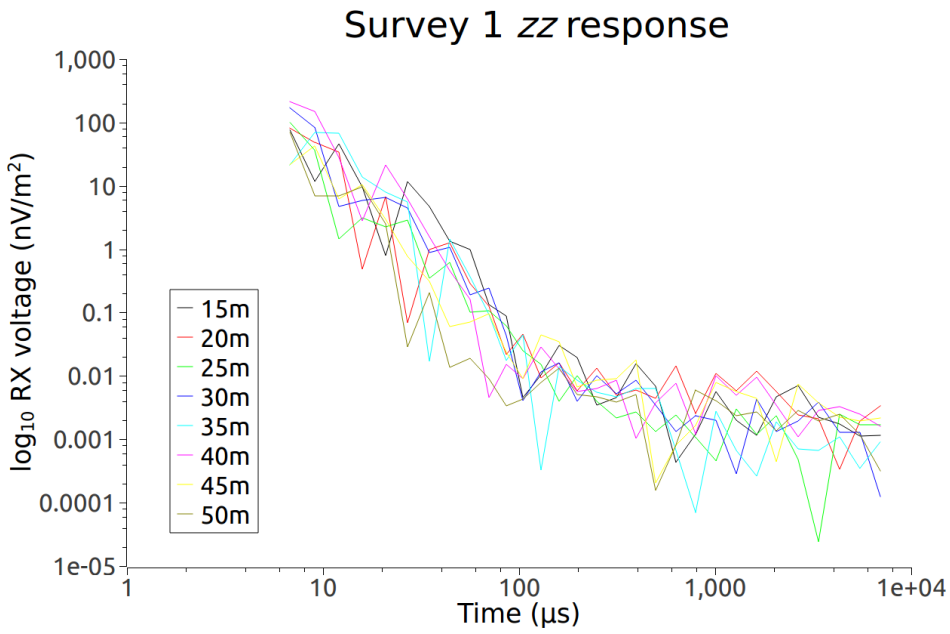

(a)

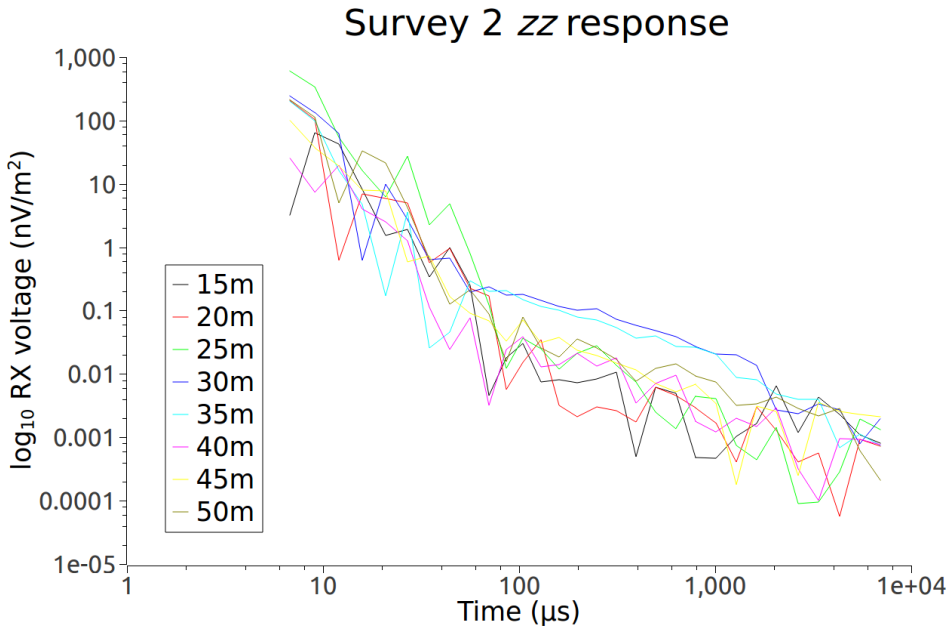

(b)

Figure 5.2: The figure shows the logarithmic value of the response for the zz component at various offsets for both surveys. The cusp in the theoretical response in Figure 5.1 occurs before the first time gate of 6.8 μs for all offsets and therefore is not present in the acquired data set.

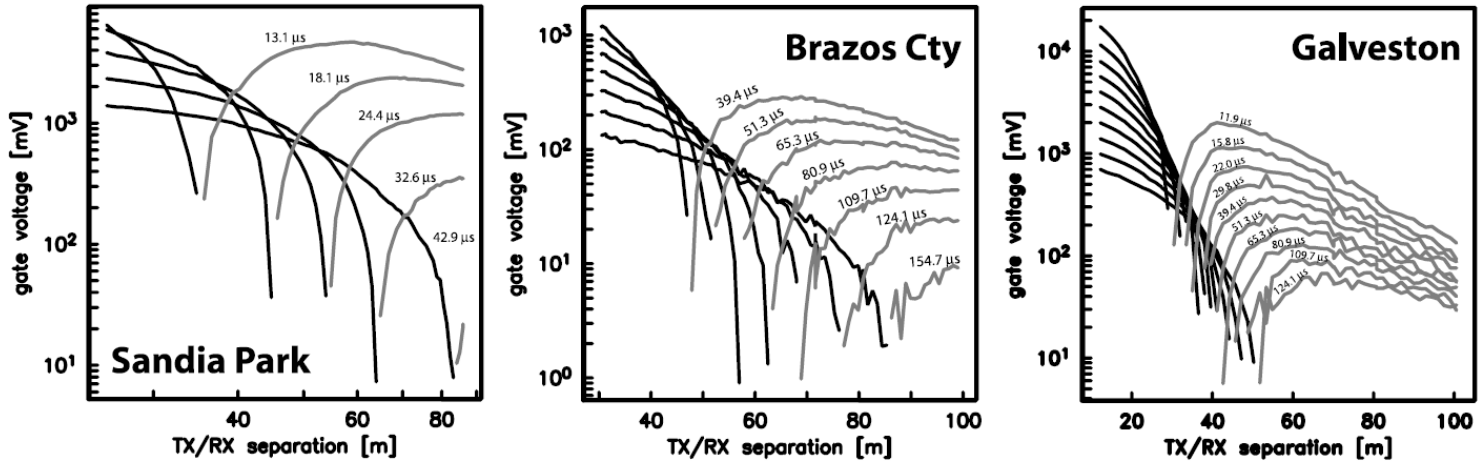

Figure 5.3: The figure shows TEM47 response curves from Sandia Park, NM, Brazos City, TX, and Galveston, TX. All three of these surveys were done over a conductive subsurface geology (From Weiss & Everett 2007).

All measured responses at times after the first 10 time gates appear to be dominated by noise as seen in the erratic nature of the responses at gates 11-30 in Figure 5.2 (a). Figure 5.2 (b) possibly shows two distinct slopes, which would indicate a two layer system. However, because the other components show high variability in the response after gate 10 and the responses after gate 10 are very small only the first 10 time gates were considered. The late-time slope, γ, of the data was computed by fitting a least-squares linear regression to the logarithmic value of the EM response versus the logarithmic value of the time after ramp-off of the transmitter for the first 10 time gates.

Figure 5.4 shows the late-time slope for the *zz*, or the horizontal coplanar, component of the EM data tensor. The TX and RX loops are highly coupled when deployed in this configuration and should have a relatively high SNR. Both surveys show γ values relatively close to the classically predicted $-5/2$ at 15 m offset. Stepping out to longer offsets there is an overall downward trend of the late-time slope in both surveys, i.e. γ decreases with increasing offset.

Another strongly coupled component of the EM tensor is the *xx*, or coaxial, component. Figure 5.5 shows the γ values for the *xx* responses for both surveys. Similar to the *zz* component, there is a general trend of decreasing γ with offset, which further suggests an increase in the roughness of the subsurface at greater depth. In addition, there is an almost quadratic shape to the late-time slope versus offset of the *xx* component for survey 2, especially for TX-RX offsets 20 - 40 m.

Finally, the *yy*, or vertically coplanar, component is shown in Figure 5.6. The *yy* EM response is most sensitive to the near surface geology. The *yy* component is not as well coupled as the *zz* or *xx*, therefore the SNR of the *yy* response will be lower. The *yy* case has a more pronounced quadratic shape to the late-time slope versus offset.

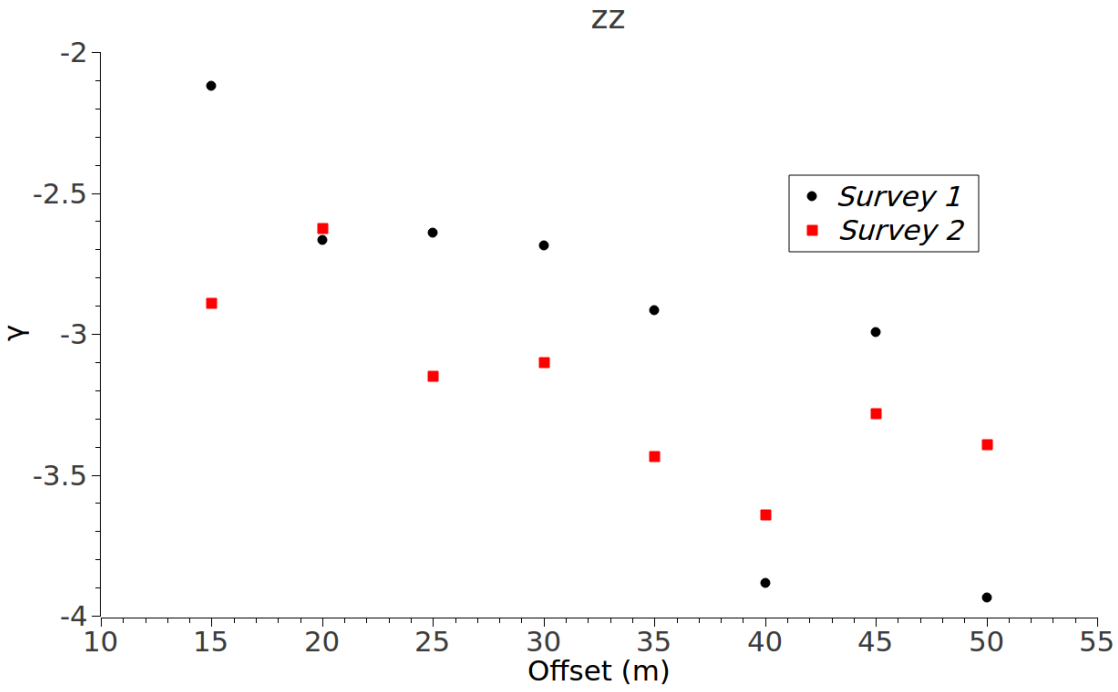

Figure 5.4: The figure shows the late-time slope of the zz component of the EM tensor versus offset for both surveys. There is a general downward trend for each survey, i.e. γ decreases with offset.

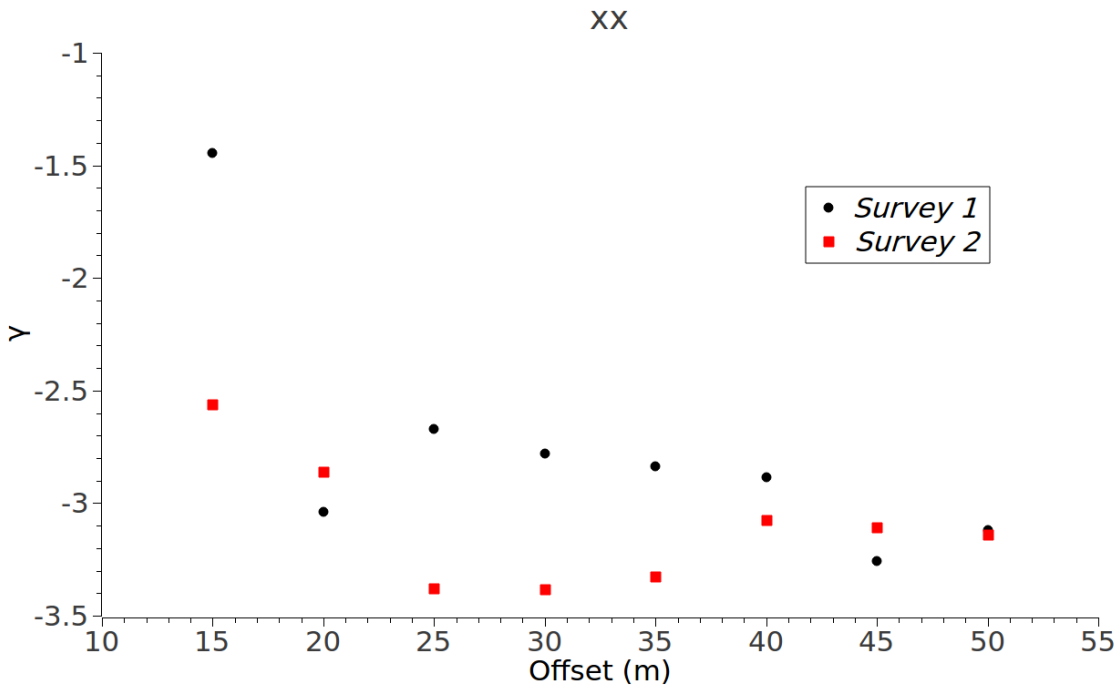

Figure 5.5: The figure shows the late-time slope γ of the xx, or coaxial, component of the EM tensor.

The off-axis elements of the EM tensor, such as the xz and xy, are more weakly coupled than the previously discussed components. Figure 5.7 and Figure 5.8 show the xz and zx late-time slopes for both surveys. The response for these components is low compared to the level of noise in the measurements and there is no apparent trend to the data.

Figures 5.9 and 5.10 show an average of the magnitude of the first three time gates at various offsets. Survey 2 (Figure 5.10) is more consistent, probably because the source was on the more conductive sandstone. Electromagnetic transient responses are generally more stable in cases where the TX loop is located over a more conductive subsurface. The induced current in a more conductive medium produces a larger response than an induced current in a resistive medium. Both surveys 1 and 2 show

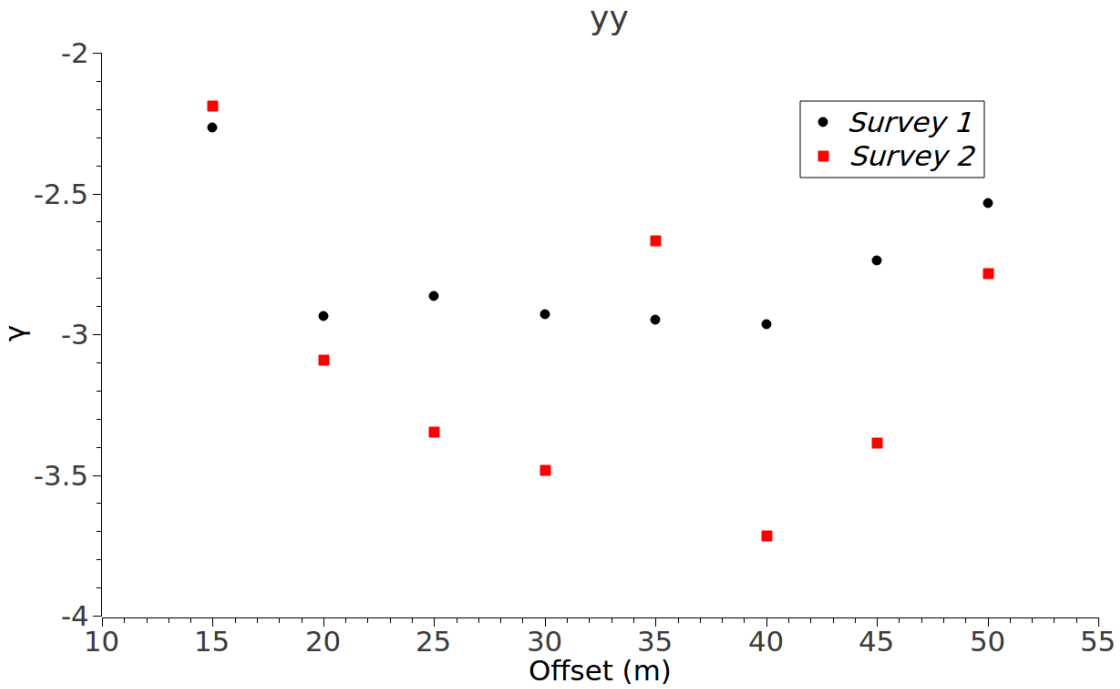

Figure 5.6: The figure shows late-time slope of the *yy*, or vertical coplanar, component of the EM tensor.

an increase in magnitude around 20 - 25 m offset. This could be because the first few time gates of the near offset sites are actually on the part of the theoretical curve (Figure 5.1) that is increasing just after the cusp. The 20 - 25 m offset range does approximately correspond to the fault core. Another possibility is that the large increase in magnitude could be a result of the lateral discontinuity at this location.

5.2 Data interpretation

The electromagnetic data from Mason, TX were used to draw conclusions about the structure of the fault zone. The EM responses at various offsets and with different orientations can be used to determine the roughness of the medium. By determining the roughness of the medium, some structural properties of the subsurface can be inferred.

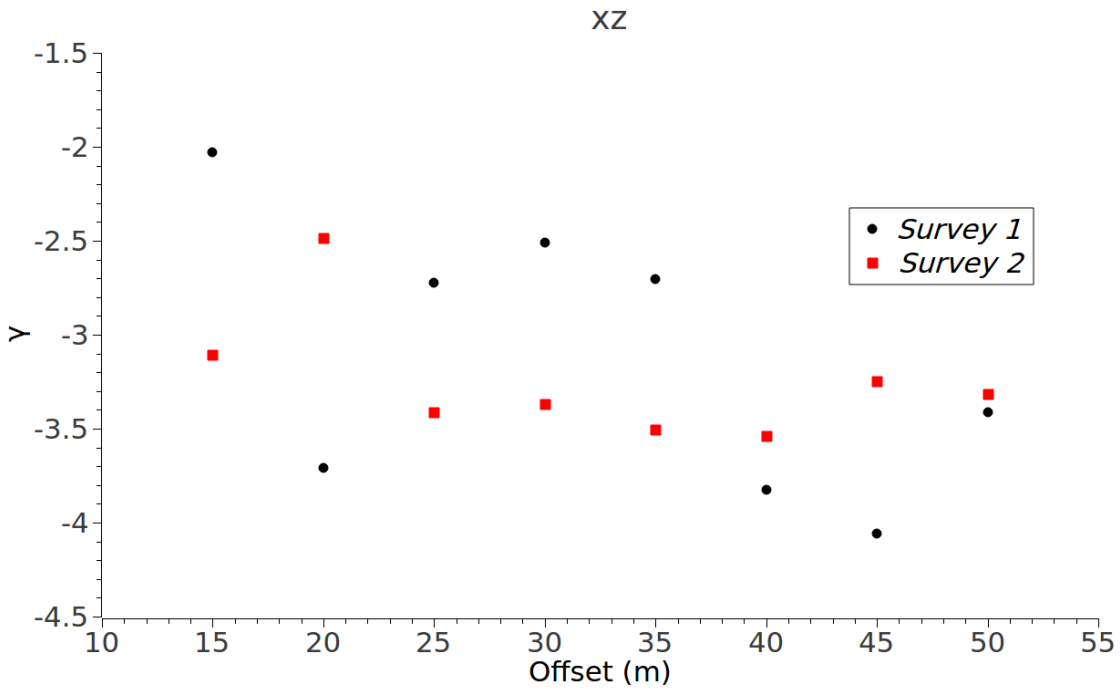

Figure 5.7: The figure is late-time slope of the xz component of the EM tensor. This arrangement is weakly coupled and there is no discernible trend to the data.

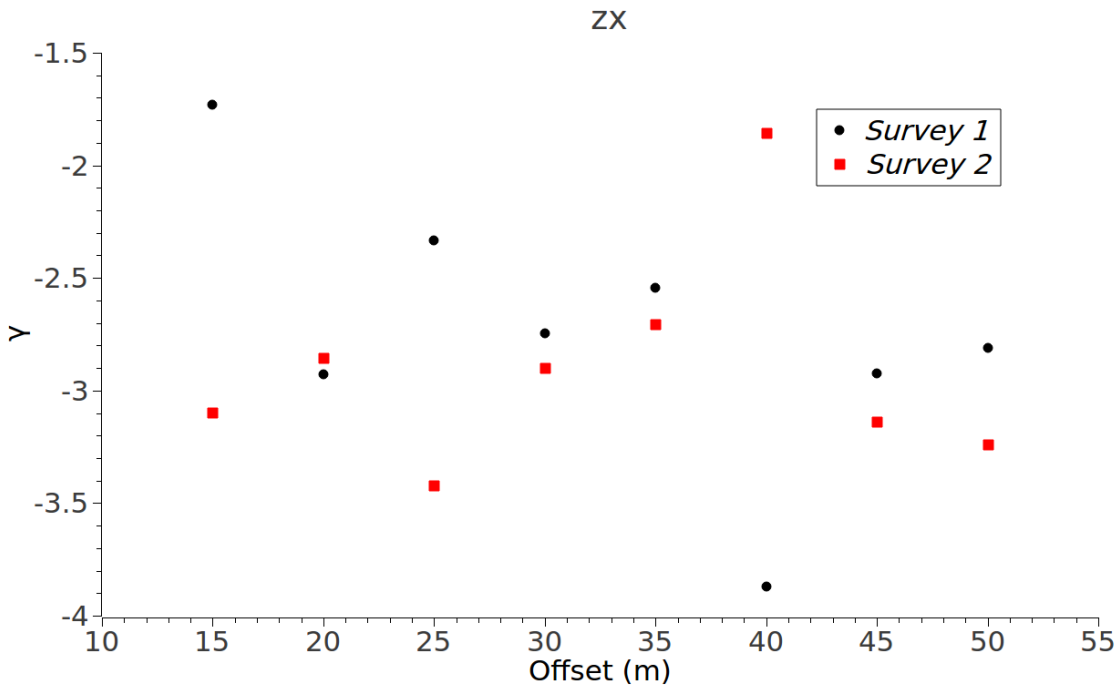

Figure 5.8: The figure is the late-time slope versus offset of the zx component of the EM tensor.

In the particular case of a homogeneous subsurface, after the ramp-off of the current in the transmitter the eddy currents diffuse downward and outward according to equations 5.1 and 5.2. The electric eddy currents generating the EM response at far TX-RX offset will be deeper in the subsurface than those at near offset. Therefore, the late-time slope response shown in previous figures is more sensitive to deeper geological features at farther offset.

Both the zz and xx components, Figures 5.4 and 5.5 respectively, show a late-time slope, γ, that decreases with increasing offset. This downward trend suggests a significant increase in the roughness of the medium as a function of depth. As previously discussed, the fault zone is expected to have numerous fractures in the subsurface. One possibility for the increased roughness at depth is that the deep

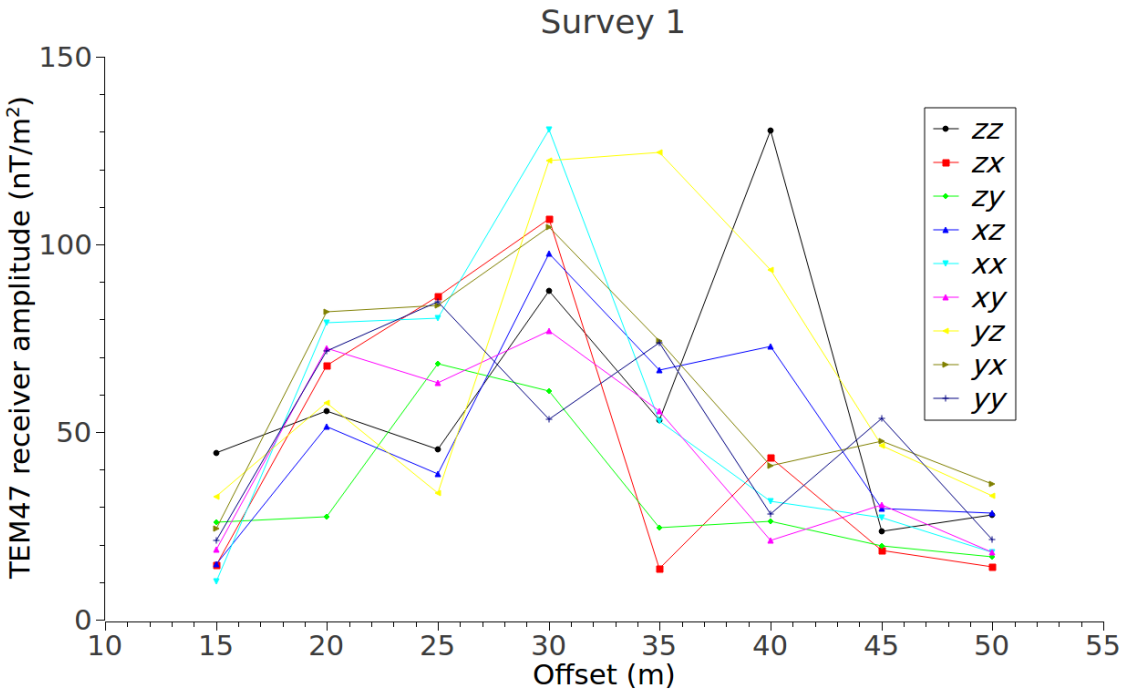

Figure 5.9: The figure shows the average of the first three time gate measurements for various offsets for survey 1.

fractures in the damage zone are filled with air. The climate in Mason, TX is mostly dry with yearly precipitation of or below 75 cm per year, so there is a high probability that that there are air-filled fractures in the deeper subsurface (Randolph 1991). These air-filled fractures would effectively be highly resistive planar features that are parallel and oriented $30° - 60°$ to the fault, and which would greatly increase the roughness of the medium. Another possibility is that there are deep fractures in the subsurface, particularly in the granite footwall, that are filled with quartz veins. Quartz filled fractures would be more resistive than the surrounding rock and would also be a cause for an increased roughness of the medium. Fractures surfaces are also "rough" and their spacing distributions are power-law distributed which would also account for the roughness in the response.

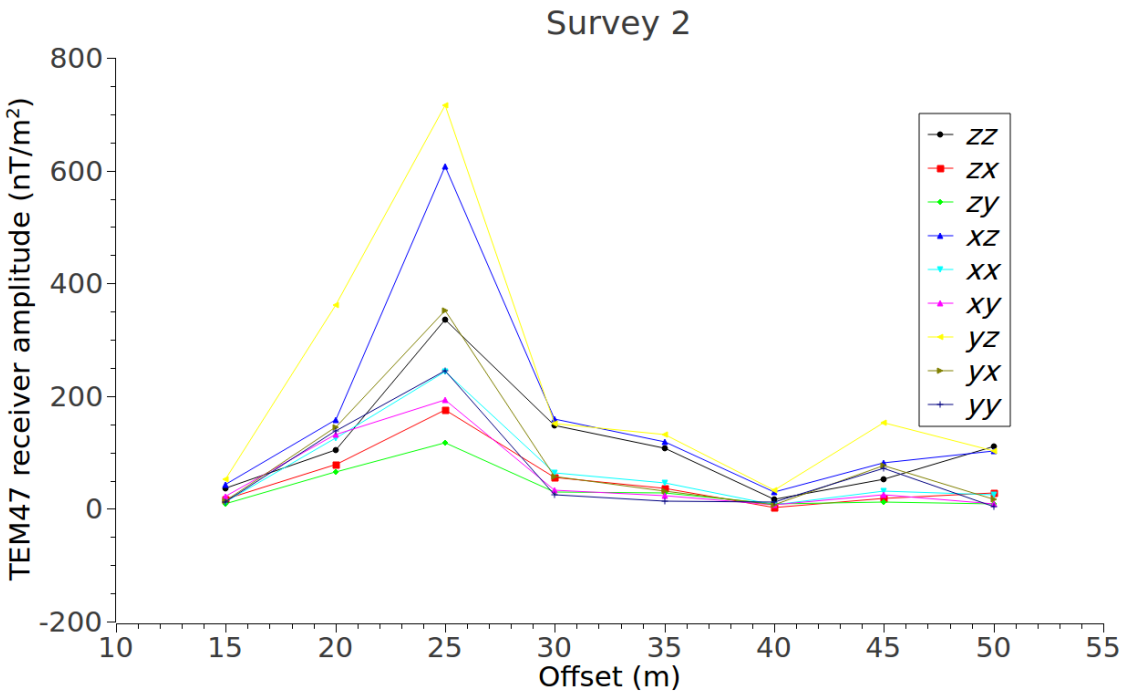

Figure 5.10: The figure shows the average of the first three time gate measurements for various offsets for survey 2. The response is more consistent than in survey 1, most likely because the source is over the more conductive Hickory sandstone.

The yy component of the EM tensor shown in Figure 5.6 is more sensitive to the shallow subsurface. For both survey 1 and 2 the late-time slope at 15 m offset is above the classical $\gamma = -5/2$ indicating that the very near surface on both sides of the fault is conductive. This is most likely to due to the weathered layer in the area being more conductive than the underlying rock. In addition the late-time slope response dips in the mid-offset range, 20 - 40 m, which suggests an increase in roughness. Even though the fractures in the near surface of the fault zone are more likely to be filled with soil, which would increase the conductivity of the fracture planes, these would likely increase the apparent roughness. An alternative explanation would be that this range is also over a local topographic high. The increased roughness indicated by the yy component could be due to a lack of soil covering the rock in that particular area. For both surveys the γ value increases back towards the classical $-5/2$ at long offset. This is likely because the late-time response on the other side of the fault will be determined by regions of subdiffusion on either side o the fault averaging with a region of superdiffusion within the fault zone.

A further interesting observation regarding the zz, xx, and yy responses, Figures 5.4, 5.5, and 5.6 respectively, is that in almost all cases the γ value for survey 1 is less than the γ value for survey 2. Intuition would suggest that survey 2, with the transmitter over the more conductive Hickory sandstone hangingwall, would provide a smoother medium and therefore have lower overall γ values than survey 1 in which the transmitter is over the more electrically resistive granite footwall. However, looking at Figures 5.4, 5.5, and 5.6 the opposite appears to be true, even for 15 m offset which is outside of the fault zone. At the time of writing this can still not be explained.

6. SUMMARY

Several electromagnetic surveys were conducted over a Pennsylvanian aged fault in central Texas to characterize the subsurface structure of the fault as well as study the diffusive behavior of induced electric currents in a fractured medium. The field site is over a high angle, oblique-slip fault along a granite-sandstone contact. The fault zone is approximately 20 m wide where surveyed and is characterized by numerous fractures.

The roughness, which we presume is a proxy of the subsurface fracture density was determined by a 2-dimensional data set that recorded all 9 components of the electromagnetic response tensor. The roughness increased with transmitter-receiver offset, which suggests the roughness increases with depth. These larger roughness values possibly indicate highly resistive fractures in the subsurface. Lower roughness values at near offset and for the yy coupled system suggest more electrically conductive fractures near the surface.

In hindsight I can recommend some changes to the survey methodology that would improve and refine this study. Since the geology in the field site has such a low conductivity, the early response and zero-crossing time are not seen because they occur before the first time gate in the electromagnetic response surveys. Therefore, the source loop should be moved further from the fault in order to capture the early response and zero-crossing time over the fault zone. Future electromagnetic work in this area should consider the highly resistive subsurface and alter the survey geometry as necessary. In addition, an electromagnetic survey along the strike of the fault should be conducted to provide more information regarding the anisotropic nature of the subsurface.

The 3-dimensional and azimuthal surveys should be repeated using an 120 s integration time to improve the SNR and the 3-component source and receiver to measure the 9 component electromagnetic tensor. This would be time intensive as it would greatly increase the acquisition time for each site compared to previous surveys. However, it would provide a much better SNR than previous measurements, and the different orientations would provide a more complete data set over the fault zone.

REFERENCES

Amara, A., 2015, Multi-input/multi-output GPR acquisition in Mason, Texas (to appear): Ms thesis, Texas A&M University.

Amsburry, D. L. and W. T. Haenggi, 1993, Middle Pennsylvanian strike-slip faulting in the Llano Uplift, central Texas, Bulletin Houston Geological Society.

Barnes, V.E. and W. C. Bell, 1977, The Moore Hollow Group of Central Texas: The University of Texas at Austin, Bureau of Economic Geology, Report of Investigations no. 88, p. 169

Becker, J. E., 1985, Structural analysis of the western Llano uplift with emphasis on the Mason fault: Ms thesis, Texas A&M University.

Ben-Zion, Y. and C. G. Sammis, 2003, Characterization of fault zones, Pure Applied Geophysics, vol. 160, p. 677-715.

Collins, J. L., 2004, Detection of near-surface anisotropy in a weathered metamorphic schist using time-domain electromagnetics: Ms thesis, Texas A&M University

Chester, F.M., J.S. Chester, D.L. Kirschner, S.E. Schulz, and J.P Evans, 2004, Rheology and deformation in the lithosphere at continental margins, Columbia University Press, New York.

Cohrs, F. F. R., 2012, Seismoelectric imaging of a shallow fault system employing

fault guided waves: Ms thesis, Texas A&M University.

Dalziel, I. W. D., Mosher, S. and L. M. Gahagan, 2000, Laurentia-Kalahari collision and the assembly of Rodinia, The Journal of Geology, vol. 108, p. 499-513.

Decker, K. T. and M. E. Everett, 2009, Roughness of a layered geological medium and implications for interpretation for the transient electromagnetic response of a loop source, Society of Exploration Geophysicists, Symposium on the Application of Geophysics to Engineering and Environmental Problems.

Duba, A., Piwinskii, A. J., Santor, M., and H. C. Weed, 1978, The electrical conductivity of sandstone, limestone and granite, Journal of Geophysical Research, vol. 53, p. 83-597.

Everett, M. E. (2009), Transient electromagnetic response of a loop source over a rough geological medium, Geophysics Journal International, vol. 177, p. 421-429.

Everett, M. E., Collins, J. L. and B. Johnson, 2006, Detection of near-surface horizontal anisotropy in a weathered metamorphic schist at Llano Uplift (Texas) by transient electromagnetic induction, Physics of the Earth and Planetary Interiors, vol. 158, p. 159-173.

Fossen, H., Schultz, R. A., Shipton, Z. K. and K. Mair, Deformation bands in sandstone: a review, Journal of the Geological Society, vol. 164, 2007, p.

755-769.

Giordano, N. J. and H. Nakanishi, 2006, Computational Physics-2nd ed., Pearson Prentice-Hall.

Grandjean, G. and J.C. Gourry, 1996, GPR data processing for 3D fracture mapping in a marble quarry (Thassos, Greece), Journal of Applied Geophysics, vol. 36, p. 19-30.

Griffiths, David J., 1996, Introduction to Electrodynamics- 3rd ed., Prentice-Hall.

Guo, W.J., Wang, Y.X., Xie, M.X. and Y.J. Cui, 2009, Modeling oil spill trajectory in coastal waters based on fractional Brownian motion, Marine Pollution Bulletin, vol. 58, p. 1339-1346.

Helper, M., 2006, Geologic map of the Mason mountain w.m.a, Mason co., Texas.

Merrill, Glen K. et al., 1991, Introduction to the Llano Uplift region. Carboniferous geology and tectonic history of the southern Forth Worth (Foreland) basin and Concho platform, Texas, p. 1-2.

Metzler, R. and J. Klafter, 2000, The random walk's guide to anomalous diffusion: A fractional dynamics approach, Physics Reports, vol. 339, p. 1-77.

Nabighian, M. N., 1979, Quasistatic transient response of a conducting half space: An approximate representation, Geophysics, vol. 44, no. 10, p. 1700-1705.

Pereira, A., 2013, Geophysical fault mapping using the magnetic method at Hickory Sandstone aquifer, Llano Uplift, Texas: Ms thesis, Texas A&M University.

Protem 47D Operating Manual for 20/30 Gate Model, 2006, Geonics Limited.

Randolph, L. C., 1991, The effects of faults on the groundwater system in the Hickory Sandstone aquifer in central Texas: Ms thesis, Texas A&M University.

Saslow, W.M., 1992, Maxwell's theory of eddy currents in thin conducting sheets, and applications to electromagnetic shielding and MAGLEV, American Journal of Physics, vol. 60, p. 693-711.

Satti, S. A., 2000, Integrated geophysical study of near-surface faults in the Wilcox Group, Texas, with application to lignite mining: MS thesis, Texas A&M University, College Station, Texas.

Scher, H. and E. W. Montroll, 1975, Anomalous transit-time dispersion in amorphous solids, Physical Review B, vol. 12, no. 6.

Smith, R.K., and W. Gray, 2011, Geochemistry and petrogenesis of Mesoproterozoic ($\tilde{1}$.1 Ga) magmatic enclaves in granites of the eastern Llano Uplift, central Texas, USA, Lithos, vol. 125, p. 463-481.

Teran, I. A. P., 2007, Stratal architecture and sedimentology of a portion of the Upper Cambrian Hickory Sandstone, central Texas, U.S.A: MS thesis, Texas A&M University, College Station, TX.

Torabi, A., Fossen, H. and A. Braathen, 2013, Insight into petrophysical properties of deformed sandstone reservoirs, AAPG Bulletin, vol. 97, no. 4, p. 619-637.

Weiss, C. J., and M. E. Everett (2007), Anomalous diffusion of electromagnetic eddy currents in geological formations, Journal of Geophysical Research, vol. 112.

Ward, S.H. and G.W. Hohmann, 1987. Electromagnetic theory for geophysical applications, in Electromagnetic Methods in Applied Geophysics, vol. 1, p. 131-311, ed. Nabighian, M.N., SEG Press, Tulsa, OK.